R/D5232-EE-01-F

(2)

GROWTH OF HgZnTe LAYERS BY LPE TECHNIQUE

Final Report

by

A. Sher, A. Tsigelman and D. Eger

March 1988

United States Army

EUROPEAN RESEARCH OFFICE OF THE U.S. ARMY

London England

Contract Number DAJA45-85-C-0049

SOREQ NUCLEAR RESEARCH CENTER

Unclassified
SECURITY CLASSIFICATION OF THIS PAGE

ADA198368

REPORT DOCUMENTATION PAGE

Form Approved
OMB No 0704-0188
Exp Date Jun 30, 1986

1a. REPORT SECURITY CLASSIFICATION Unclassified	1b. RESTRICTIVE MARKINGS
2a. SECURITY CLASSIFICATION AUTHORITY	3. DISTRIBUTION/AVAILABILITY OF REPORT Approved for public release; distribution unlimited
2b. DECLASSIFICATION/DOWNGRADING SCHEDULE	
4. PERFORMING ORGANIZATION REPORT NUMBER(S)	5. MONITORING ORGANIZATION REPORT NUMBER(S) R&D 5232-EE-01
6a. NAME OF PERFORMING ORGANIZATION Soreq Nuclear Research Center Israel Atomic Energy Commissio	6b. OFFICE SYMBOL (If applicable)
6c. ADDRESS (City, State, and ZIP Code) Yavne 70600 Israel	7a. NAME OF MONITORING ORGANIZATION USARDSG(UK)
	7b. ADDRESS (City, State, and ZIP Code) Box 65 FPO New York 09510-1500
8a. NAME OF FUNDING/SPONSORING ORGANIZATION USARDSG(UK) ERO	8b. OFFICE SYMBOL (If applicable) AMXSN-UK-RI
	9. PROCUREMENT INSTRUMENT IDENTIFICATION NUMBER DAJA45-85-C-0049
8c. ADDRESS (City, State, and ZIP Code) Box 65 FPO New York 09510-1500	10. SOURCE OF FUNDING NUMBERS PROGRAM ELEMENT NO. 61102A; PROJECT NO. 1L161102BH1; TASK NO. 7 03; WORK UNIT ACCESSION NO

11. TITLE (Include Security Classification)

(U) Growth of HgZnTe Layers by the LPE Technique

12. PERSONAL AUTHOR(S)
A. Sher, A. Tzigelman, D. Eger

13a. TYPE OF REPORT	13b. TIME COVERED	14. DATE OF REPORT (Year, Month, Day)	15. PAGE COUNT
Final	FROM 1986 TO 1988	March 1st., 1988	44

16. SUPPLEMENTARY NOTATION

17. COSATI CODES			18. SUBJECT TERMS (Continue on reverse if necessary and identify by block number)
FIELD	GROUP	SUB-GROUP	
09	01		
09	03		

19. ABSTRACT (Continue on reverse if necessary and identify by block number)

Solid solution mixtures of a wide band gap II-VI compound with one constituent being the semimetal HgTe may be tuned to yield narrow gap semiconductors, suitable for the fabrication of infrared (3μm-14μm) photon detectors. Among this group of solid solutions, $Hg_{1-x}Cd_xTe$ is at present the most commonly used material for photon detectors. Inspite of the scientific and technological achievments difficulties still exsist, generally attributed to the instability of these alloys. Thus, theoretical prediction about the relative stability of $Hg_{1-x}Zn_xTe$, reported recently, stimulated experimental research into the narrow band gap range of this solid solution.
In the present work the LPE of $Hg_{1-x}Zn_xTe$ was studied, focusing on the evaluation of this technique as a tool for

over

20. DISTRIBUTION/AVAILABILITY OF ABSTRACT XX UNCLASSIFIED/UNLIMITED XX SAME AS RPT XX DTIC USERS	21. ABSTRACT SECURITY CLASSIFICATION Unclassified
22a. NAME OF RESPONSIBLE INDIVIDUAL Dr. John M. Zavada	22b. TELEPHONE (Include Area Code) 01-402 4423
	22c. OFFICE SYMBOL AMXSN-UK-RI

DD FORM 1473, 84 MAR

83 APR edition may be used until exhausted
All other editions are obsolete.

SECURITY CLASSIFICATION OF THIS PAGE
Unclassified

cont'd achieving epitaxial layers of the "new material", the solid solution $Hg_{1-x}Zn_xTe$, with morphological, crystalline and electrical properties comparable with those of HgCdTe epilayers. The experimental work concentrated in three directions.

A. The relation between the growth solution, the growth process and the characterisation of the epilayers.

B. The effect of the substrate lattice mismatch on the LPE process of the HgZnTe and the role of the strain energy, originating from the lattice mismatch in the process.

C. Investigation of the effect of a post growth annealing process on the carrier concentration in the $Hg_{1-x}Zn_xTe$ $0.16 \leq x \leq 0.26$, epilayers.

In order to study the growth process, the effect of some growth parameters on the growth rate of the epilayers and on the epilayers morphology were examined. For this purpose, the epitaxial layers were grown on closely lattice matched $Cd_{1-z}Zn_zTe$ substrates, $0.2 \leq z \leq 0.3$. The growth parameters investigated were the initial degree of supercooling of the growth solution, the growth solution height and the duration of growth. From the dependence of the thickness on the duration of growth, the conditions in which the rate of growth was diffusion limited were determined. By fitting the experimental results to calculated curves using known models, the conditions in which the growth was from limited (thin) or unlimited (thick) solution were found. These results made possible the optimization of growth conditions. In addition, this study served as a starting point for the research of the substrate lattice mismatch effect on the liquid phase epitaxy of HgZnTe.

In order to study the effect of lattice mismatch, epilayers of $Hg_{1-x}Zn_xTe$, $0.16 \leq x \leq 0.24$, and of $Cd_{1-y}Zn_yTe$, $0 \leq y \leq 0.26$, were grown on $Cd_{1-z}Zn_xTe$, $0 \leq z \leq 0.26$. The range of lattice mismatch in these structures varied up to 2×10^{-2}. The influence of the lattice mismatch on the surface morphology, the interface between epilayer and substrate and the crystalline quality of the epilayers was studied. Typical phenomena were found for the growth under specific range of lattice mismatch, influenced also by the initial degree of supercooling of the growth solution. The epilayers of each of the two systems were categorized into various types, according to the effect of these two parameters on the characteristics of the epilayers. The location of the $Hg_{1-x}Cd_xTe$/CdTe heterostructure in this classification is also indicated. Systematic study of the dependence of the thickness of the epilayer on the growth conditions and comparison of the results to the lattice matched case, helped to reveal the role of the strain energy, originating from the lattice mismatch, in the liquid phase epitaxy process. Thus, the formation of the various types of layers, mentioned above, could be explained. For example conditions of large negative lattice mismatch and low degree of supercooling, led to the formation of layers categorized as type II. Typically the layers of type II were mirror-like with fairly smooth interface. The crystalline quality of such a layer was poor. It was proved that layers of type II were formed through homogeneous meltback of the substrate followed by regrowth process. Under the same conditions of growth, but with good lattice match, there was no meltback-regrowth process and the epilayer quality was limited mainly by the substrate quality.

The optical transmission and the electrical transport properties of HgZnTe epilayers were measured after growth as well as after an annealing process. Thus the effect of the annealing proceess could be revealed. The annealing conditions in which the hole concentration in p- type layers was reduced to the level of $1x10^{16}$ cm^{-3}, generally required for infrared photovoltaic detectors, were found. This value was accessible only when the epilayers were closely lattice matched with the substrates. Following this treatment, photoconductive response of HgZnTe epilayer could be demonstrated.

it is demonstrated in this report that LPE can be used for growth of epilayers of HgZnTe with tailored properties for IR photon detectors, comparable with those of HgCdTe. The effect of the substrate mismatch on the the crystalline as well as on the electrical properties of the epilayers, was found to be dominant.

→ Mercury Cadmium Telluride, Mercury Zinc Telluride. (MgZn)

Table of Contents

List of Illustrations

15. Variation of $Hg_{0.8}Zn_{0.2}Te$ epilayer thickness on growth time with the degree of supercooling of the growth solution. The solid line represents the empirical dependence on Te for the lattice matched case.
16. Etched cleaved sections of $Hg_{0.8}Zn_{0.2}Te/CdTe$. The epilayers were grown with solution supercooling of: (a) 9^oC; (b) 4^oC; (c) 2^oC.
17. Typical morphology of $Hg_{0.8}Zn_{0.2}Te$ epilayers which were grown on CdTe substrates; (a) with $\delta T_o = 9^oC$; (b) with $\delta T_o = 2^oC$.
18. The divergence of the FWHM of $Hg_{0.8}Zn_{0.2}Te$ layers, related with various values of $\Delta a/a$.
19. The amount of substrate meltback expressed by; $\delta T_2/T_s$, as a function of the square of the lattice mismatch. The line was calculated according to the theory presented in ref. 28.
20. Typical transmission spectrum of an as grown HgZnTe epilayer.
21. Typical transmission spectrum of an annealed HgZnTe epilayer.
22. Change of the transmission spectrum of following the annealing process of epilayer HZ73 (see table III).
23. Carrier concentration at 80 K of HgZnTe epilayers as a function of the annealing temperature.
24. Depth profile by SIMS of 3 non metal impurities.
25. Depth profile by standard SIMS of metal impurities
26. Depth profile by SIMS of metal impurities using the "voltage offset" technique.
27. Photoconductive spectral response of HZ86 (see table III), at 80 K.

List of Tables

1. Statement of the problem

The $Hg_{1-x}Zn_xTe$ solid solution, with $0.12 \leq x \leq 0.3$, is a new narrow gap semiconductor. According to theoretical considerations and some preliminary experimental work, this solid solution is a candidate as an alternate material to $Hg_{1-x}Cd_xTe$ for photodetection applications in the IR.

The goal of this work is to evaluate the liquid phase epitaxy as a tool for preparing $Hg_{1-x}Zn_xTe$ in quality suitable for photodetectors.

2. Background

The $Hg_{1-x}Zn_xTe$ solid solution was considered as a material for photodetectors about two decades ago. However, due to difficulties in the growth of bulk single crystals of the Hg rich part of this solid solution only very limited experimental work was done until 1984. In that year Arden Sher (1) presented his theoretical predictions that $Hg_{1-x}Zn_xTe$ should be superior to $Hg_{1-x}Cd_xTe$ which has been the currently used material for photodetection applications. In 1985 (2) we published the first results on the growth and characterization of $Hg_{1-x}Zn_xTe$ liquid phase epitaxial layers. The epitaxial layers were grown on CdTe substrates. The carrier transport properties of the as grown epilayers were similar to those of $Hg_{1-x}Cd_xTe$ when compositions with the same energy gaps were compared. Improvement of the epilayers morphology and crystallinity was achieved by the growth of the epilayers on closely matched substrates, $Cd_{0.8}Zn_{0.2}Te$ (3). First results ofannealed $Hg_{1-x}Zn_xTe$ epilayers were reported by another group (4). They also displayed an array of photoconductive detectors. Results of growth and characterization of bulk single crystals of this solid solution were also reported by the same group (5). The carrier transport properties of epilayers grown by Molecular Beam Epitaxy were studied (6). These epilayers exhibited p type conductivity with mobilities higher than ever reported for $Hg_{1-x}Cd_xTe$.

While all these experimental results make $Hg_{1-x}Zn_xTe$ an attractive material for IR detectors, much work is still needed in order to assess its performance as a photodetector.

3. Approaches

The main objective for the first year of this project was to optimize the procedures of the LPE process so that the crystallinity, morphology, the shape of the interface and the thickness would be under control.

The preliminary results indicated that all of these parameters were strongly influenced by the supercooling degree of the growth solution as well as on the Zn concentration in the $Cd_{1-y}Zn_yTe$ substrates. $Cd_{1-y}Zn_yTe$ substrates with $0.2<y<0.3$ which are lattice matched with $Hg_{1-x}Zn_xTe$ are not commercially available. Growth of bulk single crystals of $Cd_{0.8}Zn_{0.2}Te$ was thus the second objective for the first year.

The main objective of the second year was to control the electrical properties of the epilayers. The annealing in Hg atmosphere was employed in order to adjust the carrier concentration to the level generally required for photon-detectors operating in the IR region.

4. Experimental

The epitaxial layers were grown from Te solution using the horizontal slider boat system. The two main components of the system are the growth boat and the growth reactor. Their description and the role of each of them in the growth process is given in the next two sections. Following these sections, details about the growth substrates and about the source materials are given. In order to control the electrical propereties of the epilayers, a post growth annealing process is essential. The annealing apparatus and the annealing process are described in the fifth section. The last section of this chapter includes a brief description of all the methods of epilayers characterization employed in this work.

4.1 The LPE boat and the LPE process

A schematic illustration of the graphite LPE boat and the relative position of its two components in the various stages of the growth process is shown in fig. (1). The inherent problems of Hg loss from the Hg-Zn-Te growth solution were solved by compensation of Hg from HgTe sources. Due to the lack of information about the exact phase diagram of the Hg-Zn-Te solution, the Zn atoms were introduced into the growth solution only by equilibration of Hg-Te solution with a ZnTe wafer. The equilibration process is denoted in fig. (1) as stage I of the thermal cycle. The duration of this stage is about one hour. On stage II, the growth solution is removed from the ZnTe wafer and the temperature of the whole apparatus drops down to the required supercooling below the saturation temperature. On stage III, the growth solution is brought into contact with the growth substrate. In this stage, the temperature of the system remains constant or ramp cooled under the required rate. The duration of stage III is 1-80 minutes, depending on the desired epilayer thickness and on the other growth conditions. At the end of this stage, the growth solution is removed from the substrate and from the epilayer grown over it.

4.2 Reactor, heaters, vacuum and gas system.

A schematic illustration of the reactor, including the heaters, vacuum and gas flow apparatus, is given in fig. (2). The reactor is a silica tube, 40 mm in diameter. The silica tube is attached to the vacuum system which includes diaphragm pump and absorption pumps. It is also connected with a

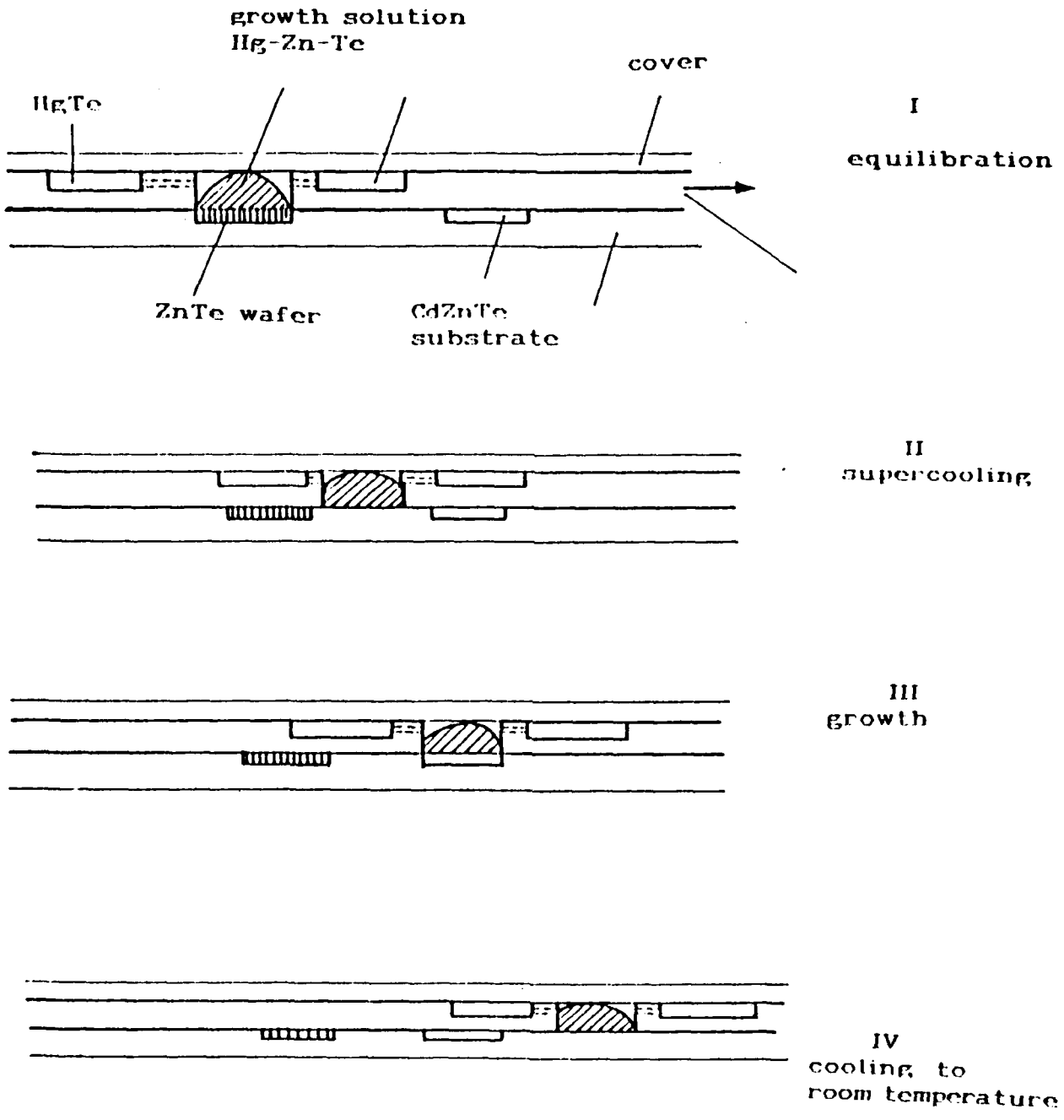

1. Schematic illustarations of the LPE boat in the various positions of the LPE process.

flow gas system of nitrogen and hydrogen. Before the growth process the reactor is evacuated and than purged with nitrogen. During the thermal cycle, Pd purified hydrogen flows through the reactor. The silica tube is located in the central axis of a cylindrical resistance heater. The temperature of the apparatus is automatically controlled and the temperature at the vicinity of the growth solution is monitored. The heater can be easily removed from the zone of the growth boat at the end of the growth process.

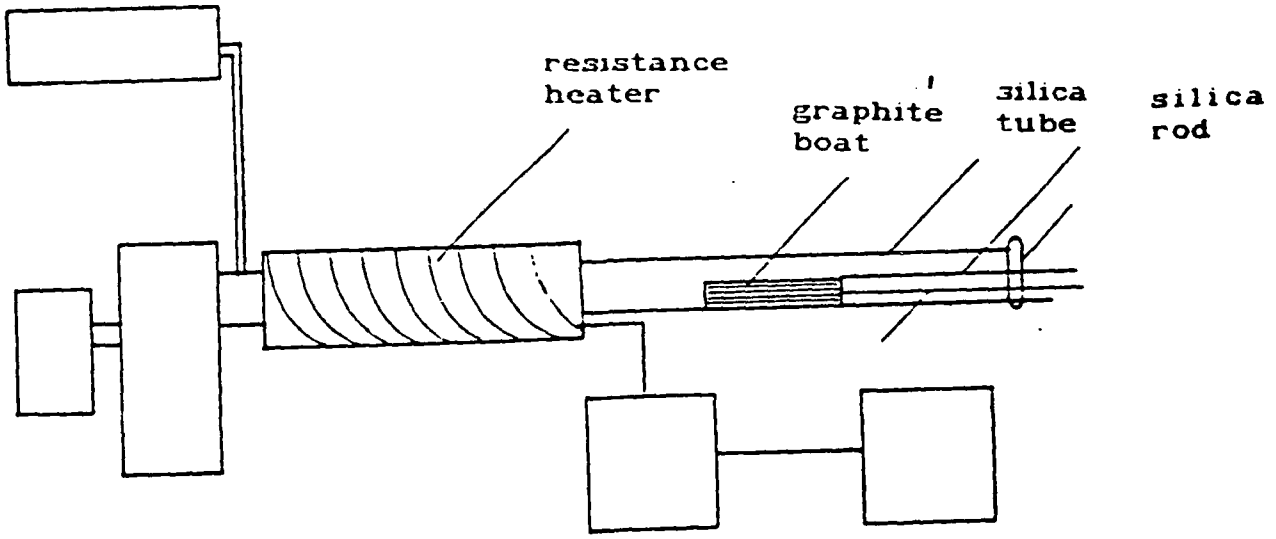

2. Schematic illustration of the LPE reactor.

4.3 Materials

The preparation of the growth solution is performed inside the growth system as a part of the growth process. The composition of the growth solution is $(Hg_{1-z}Zn_z)_{1-y}Te_y$, $y=0.80-0.85$, $z=0.01-0.02$ and the total weight of the growth solution is 1.5-3 gr. The exact composition and weight depends on the experiment requirements. All the source materials are high purity grade. The Te, the main component of the growth solution, is quadru-zone refined. A typical analysis of the trace metals in the Te, by flameless atomic absorption, is given in table I (7).

Table I: Atomic absorption analysis of tellurium

Concentration (ppm)	element
< 0.02	Ag
< 0.04	Cu
< 0.10	Al
< 0.10	Fe
< 0.10	Pb
<0.20	Sc

4.4 Growth substrates

The epilayers were grown on $Cd_{1-z}Zn_zTe$ substrates, $0<z<0.26$. Substrates with low Zn concentration were supplied by II-VI Inc. USA and by our laboratory in SNRC. For substrates with z=0.10-0.20, lattice matched with the relevant compositions of HgZnTe epilayers, single crystals were grown in our laboratory using the modified Bridgeman method. The growth procedure and typical results were described in the 3rd interim report (8). The boules were cut into wafers in the (111) direction, from which substrates of 1x1 cm^2 were diced and prepared for the growth experiments. The substrates were polished mechano- chemically with 0.02N Br-Methanol solution. Immediately prior to the LPE procedure, the contactless polishing was employed (9) in order to remove subsurface damages. The epilayers were grown, generally, on (111)B face. The B face identified by selective etching, using EAg2 solution (10); 10ml HNO_3: 20ml H_2O: 4gr $K_2Cr_2O_7$: 0.5gr $AgNO_3$.

4.5 Annealing apparatus and annealing process

The annealing process is performed in Hg atmosphere, in evacuated, sealed silica ampoules. During the annealing process the temperature of the sample, 260°C-400°C, is lower than the growth temperature. The ambient Hg pressure is much higher than in the LPE process. A schematic illustration of the annealing apparatus is given in fig. (3).

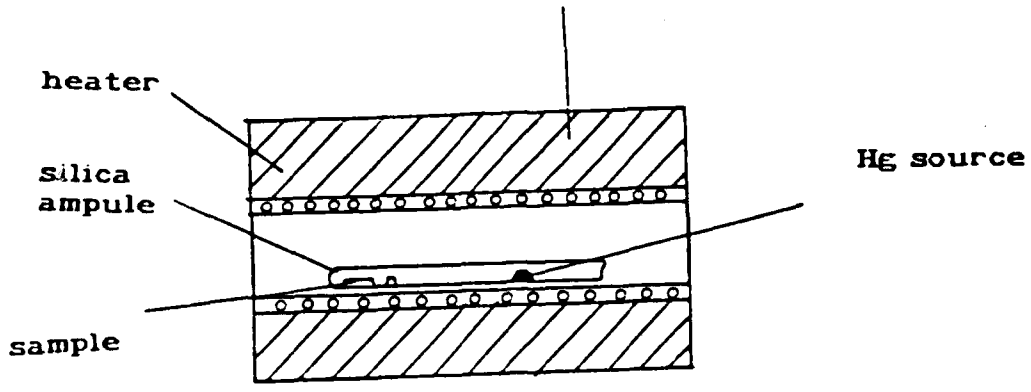

3. Schematic illustration of the annealing apparatus.

4.6 Methods of assessment

The compositions of the epilayers were determined from the FTIR transmission spectra, using the empirical dependence of the energy band gap on x (8). The thickness of the epilayers was measured by two methods: 1) Direct measurement of the thickness by optical microscope on (100) cleaved plane. 2) By measurement of the interference fringes of the transmission spectra. The morphology and the shape of the interface were characterized by optical miroscope. In order to reveal the features of the interface, Eg2 etchant (10) was used. The etchant selectively etched the $Cd_{1-y}Zn_yTe$ substrates while the $Hg_{1-x}Zn_xTe$ epilayers remained intact.

For the layers with thickness less than 10 μm the lattice mismatch between the epilayer and the substrate could be measured directly. In this case the angular separation between the x-rays diffraction peaks of the epilayer and the substrate were measured. For thicker epilayers, where the x-ray diffraction peaks of the substrate could not be detected, the lattice mismatch was evaluated by separate measurements of the x-ray diffraction angles of the epilayer and the substrate. The crystalline quality of the epilayers was determined by their x-ray rocking curve spectra using the nondispersive mode with an InSb crystal as a reference crystal.

The Hall coefficient R_H and electrical conductivity σ_o were measured by the Van der Pauw method (11) at 80 K and magnetic fields between 0.5-

10 kG. Before measurement, the wafers were cut into small samples (usually 5x5 mm^2) and then etched and rinsed using standard procedures. Four ohmic contacts were made on the sample perimeter by electroless gold plating.

In some of the annealed samples which exhibited low carrier concentration a relative photoconductive spectral response was measured. A thermal detector with a flat responsibility through the whole measurement range served as a reference detector.

5. Results and discussions

5.1 Thickness of the HgZnTe epilayers

By correlation between the epilayers thickness results and the growth conditions, the factors governing the growth rate were identified. The influence of the following parameters on the growth rate was examined: the growth duration, the initial degree of supercooling of the growth solution, the growth solution height and the temperature cooling rate during the growth process. The composition of the growth solution and the ratio between the substrate area to the growth solution area were kept constant during all these experiments. The saturation temperature was also kept constant, 470°C. In this section only the results of growth on lattice matched substrates are presented.

The dependence of epilayers thickness on the degree of supercooling of the growth solution, δT_o, is presented in fig. (4). In these experiments the

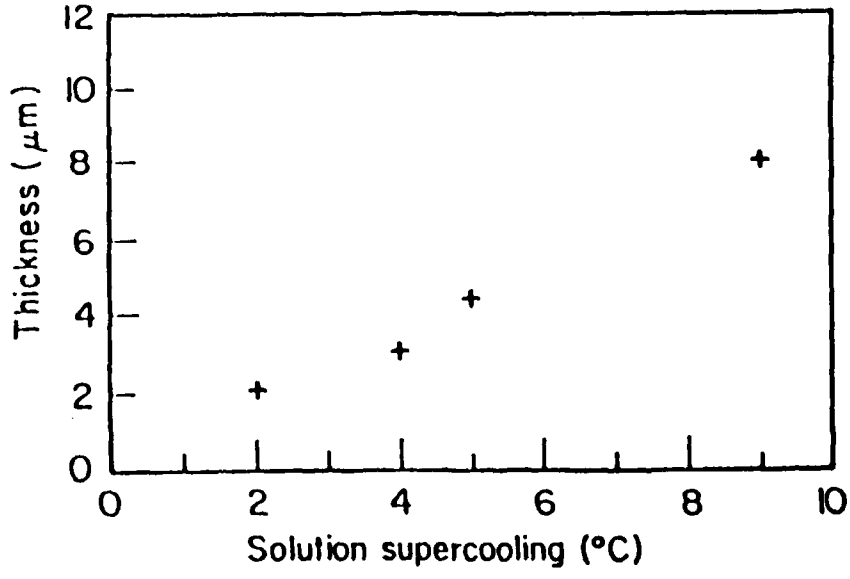

4. Variation of $Hg_{0.8}Zn_{0.2}Te$ epilayers thickeness with degree of supercooling of the growth solution.

growth was isothermal. The growth time, 40 minutes and the growth solution height, 2 mm, were kept constant. The degree of supercooling of the growth solution was intentionally changed from run to run, between 2°C to 9°C. The dependence of the thickness on the degree of supercooling was found to be linear in the examined range. The additional thickness was ~0.9 μm per one degree. The dependence of the epilayers thickness on the duration of growth is presented in fig. (5) and (6). In fig. (5) the

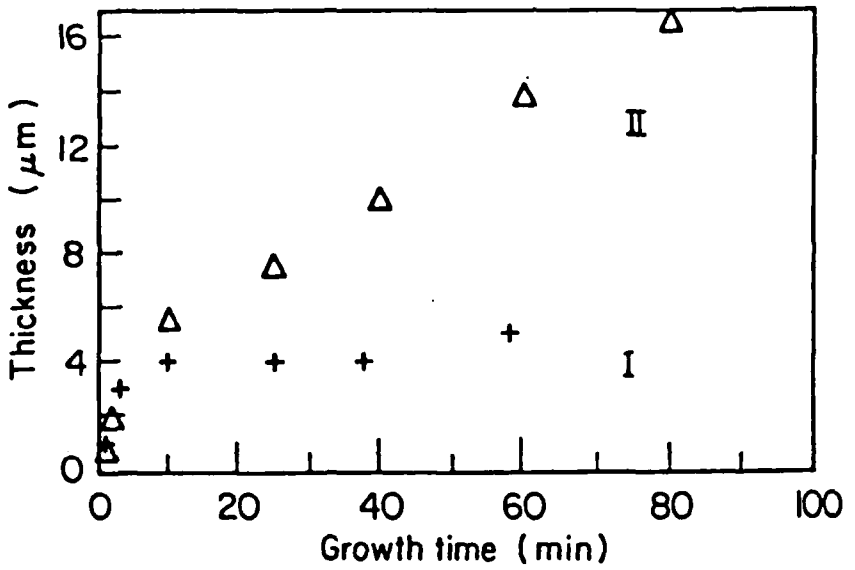

5. Variation of $Hg_{0.8}Zn_{0.2}Te$ epilayers thickness with growth time. I. Isothermal growth. II. Growth under low cooling rate.

results of two series of experiments are presented. In one series, the epilayers were grown isothermally from a presupercooled solution while in the other series, the epilayers were grown under constant cooling with the rate of 0.15 degrees per minute. δT_o was kept constant in all these growth runs- 5°C. As it can be seen in fig. (5), during the first moments of contact between the growth solution and the substrate, the rate of growth is quite similar in the two cases. Thus, under the isothermal growth, the epilayer reaches its final thickness after about 10 minutes. Under low cooling rate, the dependence of the thickness on time is linear. The results of a third series in which the dependence of thickness on time

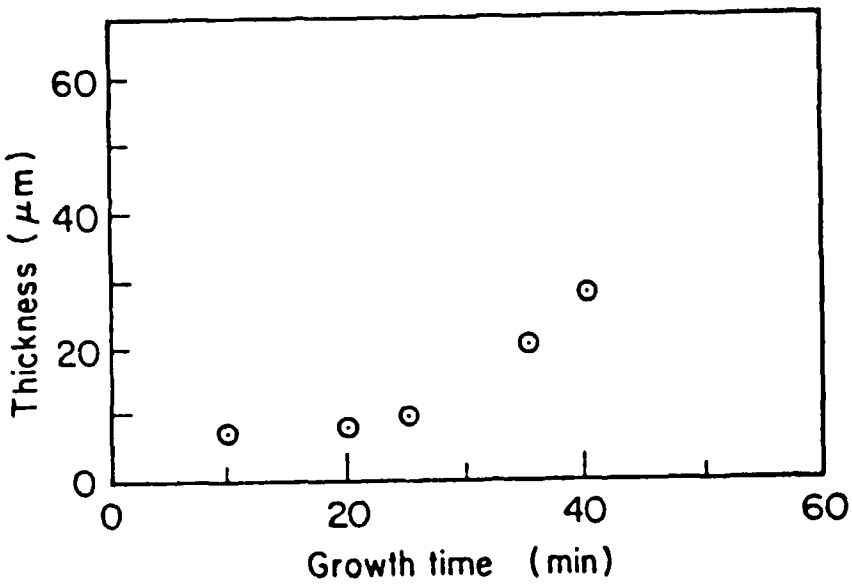

6. Variation of $Hg_{0.8}Zn_{0.2}Te$ epilayers thickness with growth time under high cooling rate.

Fig. 6

was studied is presented in fig. (6). The experiments of these series were performed under different conditions; the cooling rate during growth was raised to 0.5°C/min, the growth solution height was doubled and δT_o was 3°C. It can be seen that after long enough durations of growth the epilayers were 3 times thicker than the epilayers grown with similar duration of growth but under the conditions of the previous series. In order to examine the influence of the growth solution height, a series of growth runs in which all the growth parameters except the growth solution height were kept constant. In fig. (7) it can be seen that doubling of the growth solution height resulted in doubling of the epilayer thickness. The influence of one more parameter on the epilayer thickness, the cooling rate during growth, can be seen in fig. (8). In this series of growth runs the initial degree of supercooling, δT_o, and the amount of cooling during growth, δT_1, 3 and 12 degrees respectively, were kept constant from run to run. While for low rates of cooling, the epilayer thickness does not depend on the cooling rate, it drops steeply when the ramping rate b is raised, reaching a minimum at b = 0.7°C/min.

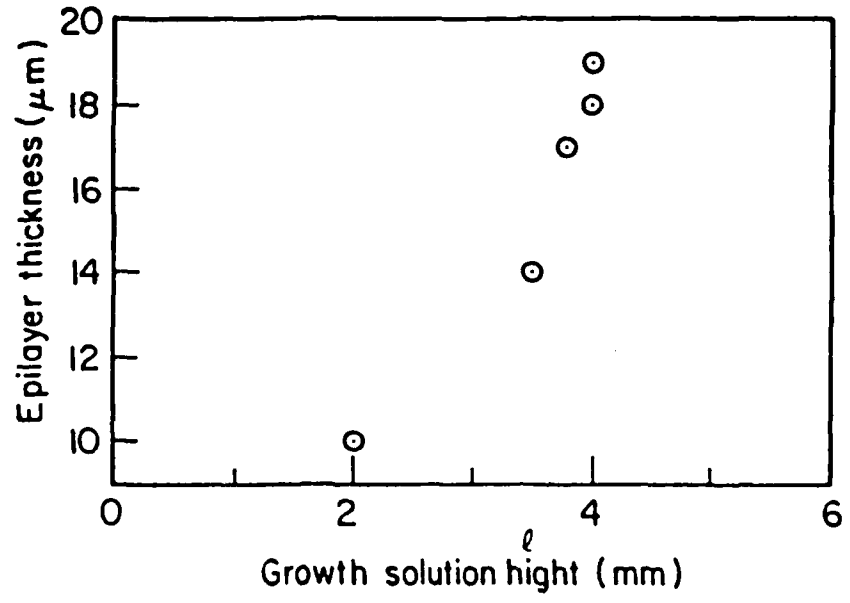

7. Variation of $Hg_{0.8}Zn_{0.2}Te$ epilayers thickness with growth solution height.

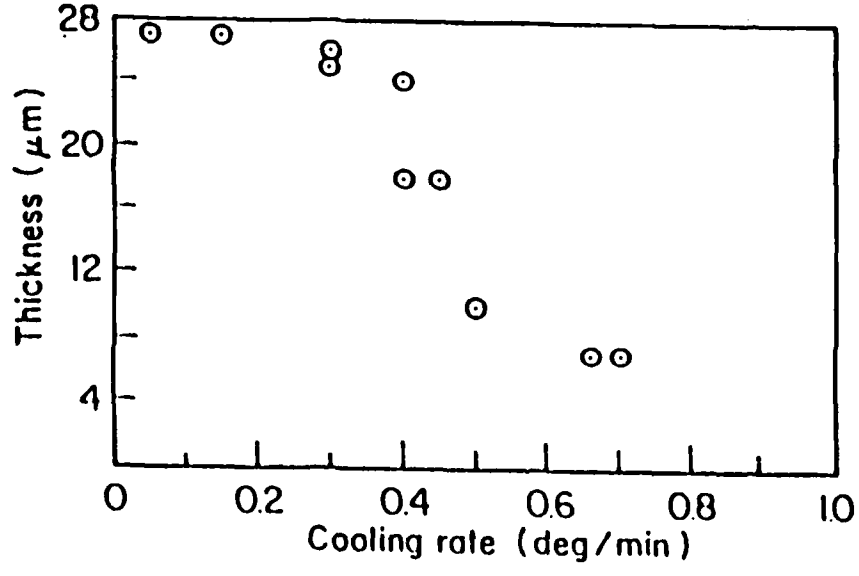

8. Variation of $Hg_{0.8}Zn_{0.2}Te$ epilayers thickness with cooling rate of the growth solution during the LPE growth.

In order to understand the experimental results it is convenient to postulate that without any limiting kinetic factors the thickness of liquid phase epitaxial layers is dependent on the deviation from equilibrium, namely, following:

$$d = C(\delta T_o + \delta T_1) \qquad [1]$$

C is constant for a specific ratio between the volume of the growth solution and the area of the substrate. In an horizontal LPE of many groups of materials, including HgCdTe, the diffusion of the solutes is the kinetic limiting factor of the growth rate (12). In multi components epilayers it can be assumed that the diffusion velocity of one of the components determines the growth rate. Considering our LPE results of HgZnTe, this assumption may be justified since the Zn concentration in the growth solution, for liquidus temperature of 470°C, is only 1/100 of the Hg concentration while its concentration in the epilayer is 1/5 of that of the Hg (4). Assuming also similar diffusion coefficients of Hg and Zn, the deposition rate of stochiometric growth units limited by the diffusion velocity of the Zn can be discussed. Well known models describe thickness dependence on isothermal growth time for two diffusion limited growth cases: 1. For the limited (thin) growth solution (13) the thickness follows:

$$[2] \quad d = \ell \delta T_o k \left[1-2 \sum_{n=o}^{\infty} \frac{\exp(-\lambda_n D t/\ell^2)}{n^4}\right] \qquad [2]$$

ℓ-growth solution height, $\lambda n = (n + 0.5)\pi$

2. For the unlimited (thick) growth solution (14) the thickness follows:

$$[3] \quad d = 2k(D/\pi)^{0.5}(\delta T_o t^{0.5}) \qquad [3]$$

The calculated epilayer thickness dependence on the growth time, for the two cases, is presented in fig. (9). The dashed line was calculated according to eq. [3] while the solid line calculated according to eq. [2]. The experimental results which have already been presented in fig. (9) fit very well to the thin solution case, with $D=8\times10^{-5}$ (15) and with $k=4.5$ μm/°C. Using the unlimited case expression, it can be seen that the calculated thickness, for growth times longer than 20 minutes, are much higher than the experimental results. The results of the growth runs performed under low rate cooling fit very well to the equations which describe the limited case under such conditions (13) as shown in fig. (10).

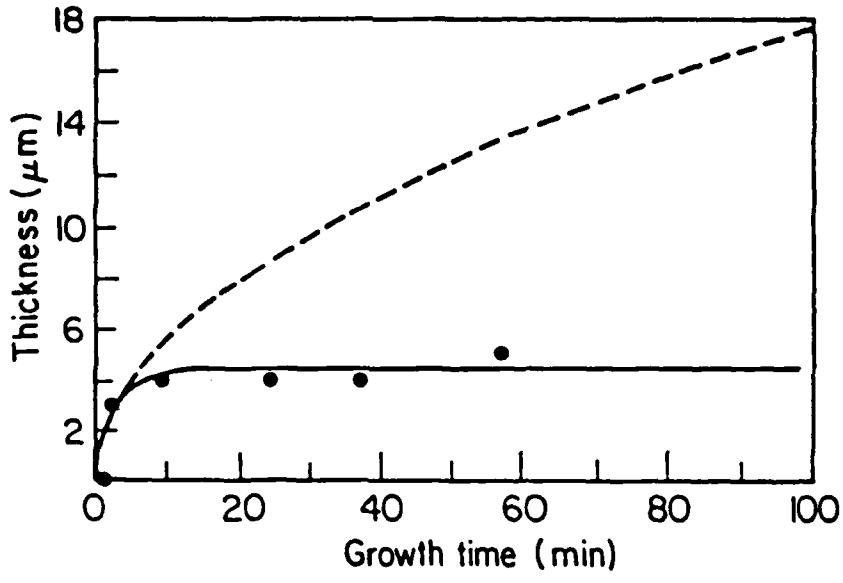

9. Calculated dependence of the epilayers thickness on growth time for isothermal growth.j Solid line - following the limited case, dashed line the unlimited case. The experimental results are those presented in fig. (5I).

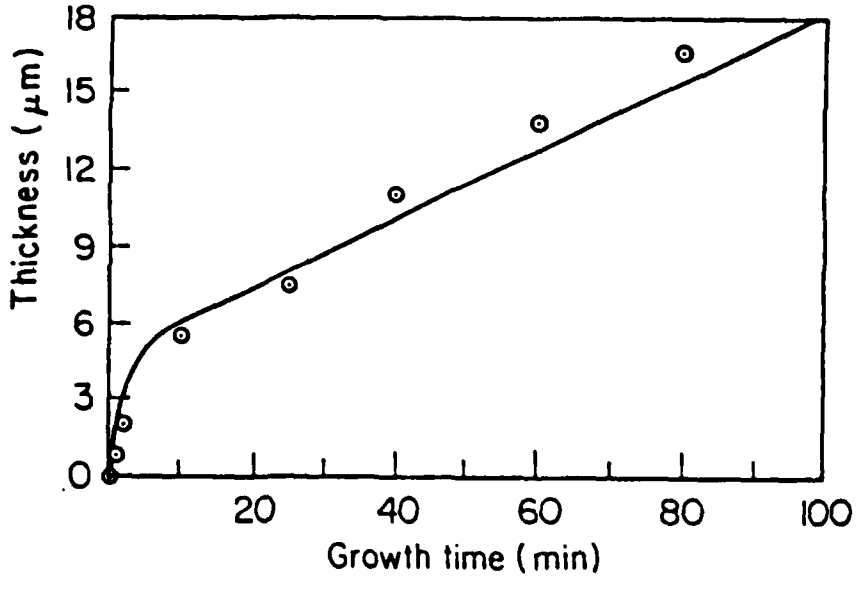

10. Calculated dependence of the epilayers thickness on growth time for low cooling rate of the growth solution. The limited case equations were used for the calculation. The experimental results are those presented in fig. (5II).

The meaning of growth from a limited solution is that after a while the epilayer reaches its equilibrium thickness following eq. [1]. This is the reason that for long enough durations of growth increasing the growth solution height resulted in thicker epilayers. On the other hand, with higher rates of cooling, the system moves from equilibrium thus the time dependence of the epilayer thickness should fit to the unlimited case (14). Such a time dependence can be seen in fig. (11). It should be

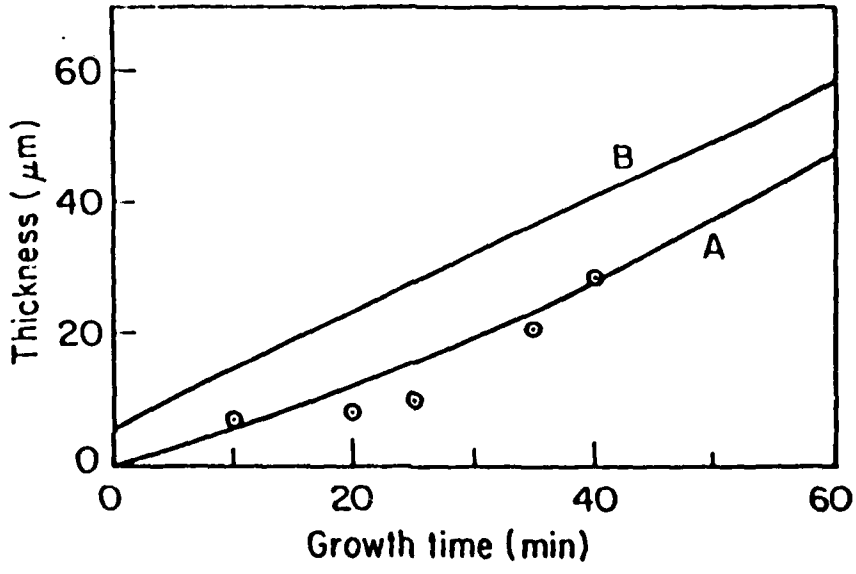

11. Calculated dependence of the epilayers thickness on growth time for high cooling rate. A. Unlimited case, the experimental results are those presented in fig. (6). B. When the diffusion limiting factor is not considered.

Fig. 11

noted that for the last fitting, the k taken into account was about 20% smaller than the k substituted for the near equilibrium cases. This difference can be explained by different growth regime since in the last case the material deposition is only from a small part of the growth solution. It should be also noted that under high cooling rates during growth, the growth rate is not diffusion limited but is controlled by surface processes kinetics (16). It may be assumed that this is the reason for the deviation of the calculated dependence of growth rate on cooling rate for high cooling rates, as it can be seen in fig. (12).

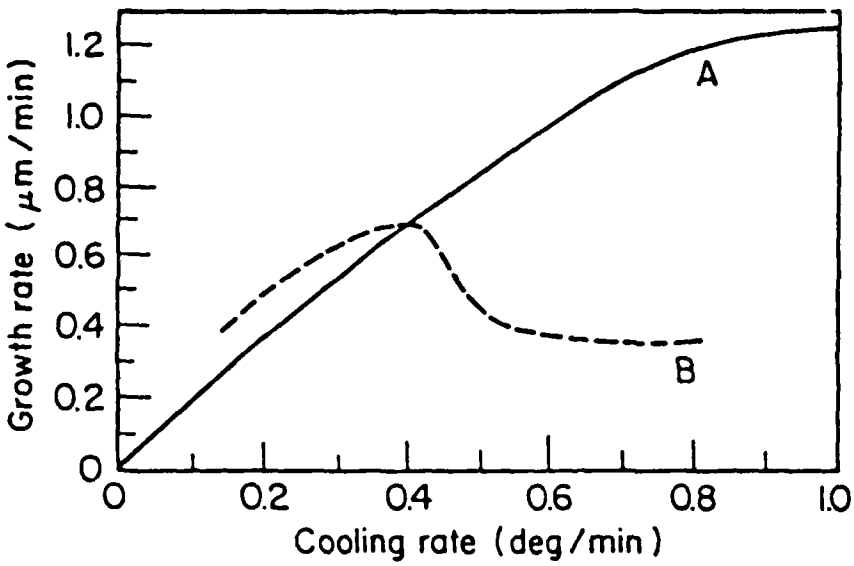

12. Calculated dependence (solid line) of the growth rate on the cooling rate of the growth solution, following the unlimited case. The dashed line is the experimental growth rate following the experimental results presented in fig. (8).

Fig. 12

5.2 The influence of the cooling rate during growth on the epilayers morphology.

The influence of the cooling rate during growth on the epilayers morphology can be seen by comparison between fig. (13) to fig. (14). The morphology of an epilayer grown under a low cooling rate, 0.15°C/min, is seen in fig. (13a). The morphology is undulant, typical to LPE growth, with no interfering to the epilayer continuity. By looking at the cleaved cross section of this epilayer, fig. (13b), it can also be seen that the epilayer is continuous and the interface is sharp. Such results were typical to all the epilayers grown on lattice matched substrates under cooling rates lower than 0.3°/min. The morphology of an epilayer grown under cooling rate of 0.7°C/min is seen in fig. (14a).

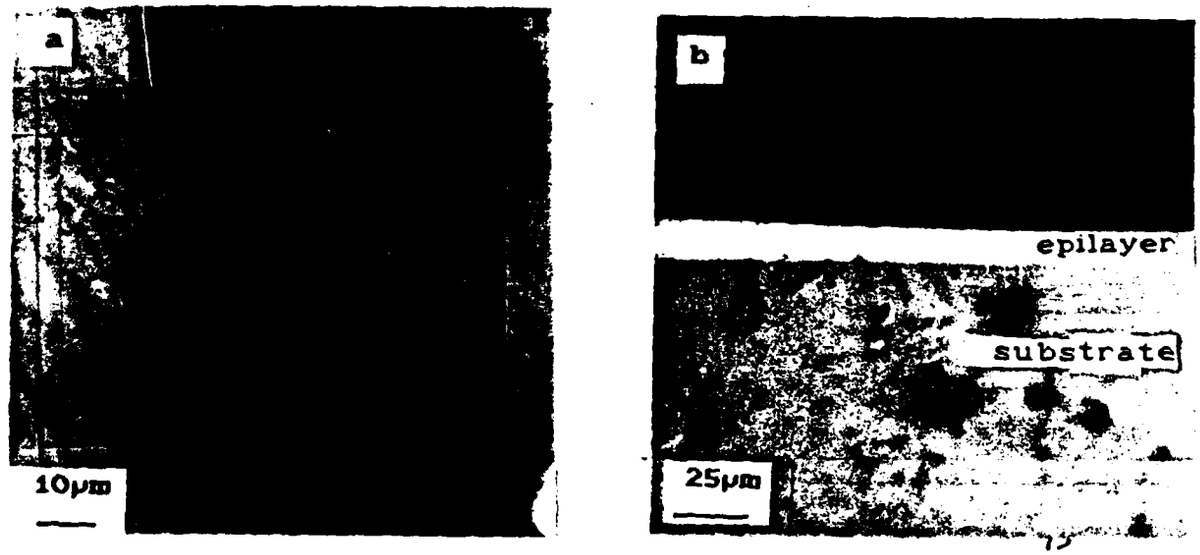

13. Morphology of HgZnTe epilayer grown on lattice matched substrate under low cooling rate (a) top view, b(110) cleaved section.

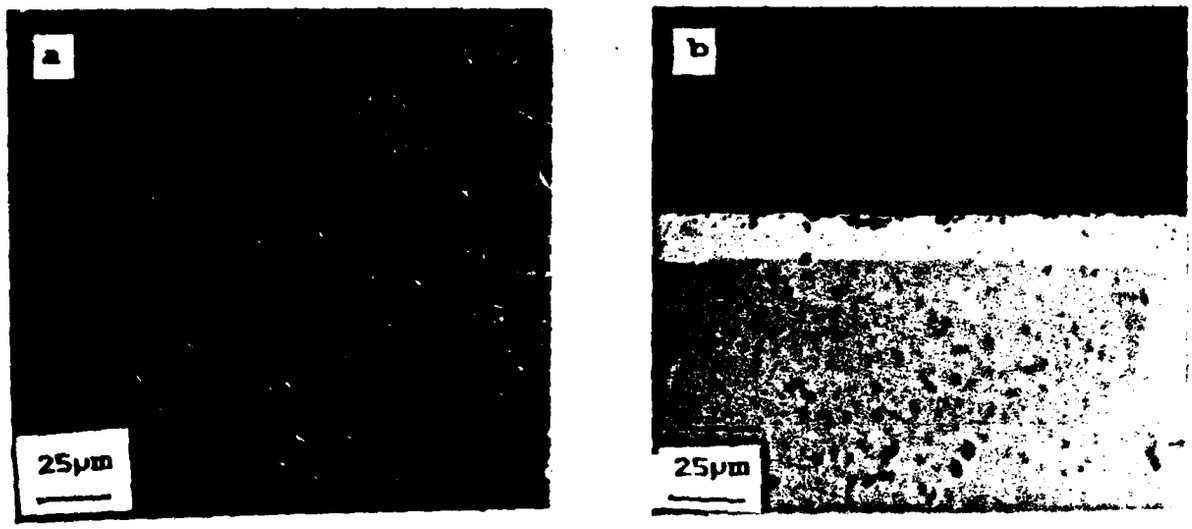

14. Morphology of HgZnTe epilayer grown on lattice matched substrate and high cooling rate (a) top view (b) (110) cleaved section.

Defects, most of them concentrated at the boundaries of longitudal cells, can be seen. Looking at the cleaved cross section of this layer, fig. (14b), it is seen that the interface is sharp but the epilayer itself, mainly at the vicinity of the free surface is disturbed. These phenomena were typical to growth under high rates of cooling. It is possible that because of the high cooling rates, the liquid close to substrate is extremely enriched in the solutes. The situation in this case is analogous to constitutional supercooling which is a well known phenomenon in the crystal growth of solid solution from a melt but less probable in LPE (16).

5.3 The effects of the substrate lattice mismatch on the LPE of HgZnTe.

The contact of supersaturated growth solutions of Hg-Zn-Te with $Cd_{1-z}Zn_zTe$ substrates, $0<z<0.26$, resulted in the growth of continuous $Hg_{1-x}Zn_xTe$ epilayers. The characteristics of the epilayers were strongly dependent on two main factors: 1. $\Delta a/a$, the lattice mismatch between the layer and the substrate. 2. δT_o, the supercooling degree of the Hg-Zn-Te solution. The influence of these two factors on the thickness of the epilayers will be discussed first.

The dependence of the thickness on δT_o for $Hg_{0.8}Zn_{0.2}Te$ epilayers grown on $Cd_{0.8}Zn_{0.2}Te$ lattice matched substrates, was presented in fig. (4). These results are presented again (circles) in fig. (15). The solid line, with a slope of 0.9 $\mu m/^oC$, fits to this set of experimental results. The new set of experimental results (triangles), presented in this figure, are of $Hg_{0.8}Zn_{0.2}Te$ grown under the same conditions but on CdTe substrates. The lattice mismatch in this case is $\sim 2\times10^{-2}$. It can be seen that for $\delta T > 5^oC$, also these experimental results fit to the linear dependence. On the other hand, for lower values of δT_o, there is an opposite dependence, the thickest epilayers are with the lowest values of δT_o. The results were similar when the epilayers were grown on $Cd_{0.96}Zn_{0.04}Te$ substrates. Some other characteristics of the epilayers, namely, morphology, shape of the epilayer - substrate interface and the crystallinity could also be categorized by these two parameters, δT_o and $\Delta a/a$. According to these parameters, the HgZnTe epilayers were classified into four types. The results are summarized in table II. The value of C in table II was derived by substituting the measured thickness into equation [1]. The shapes of the interfaces typical to the layers of types II, III and IV are displayed in fig. (16). All the epilayers were grown from growth solutions with

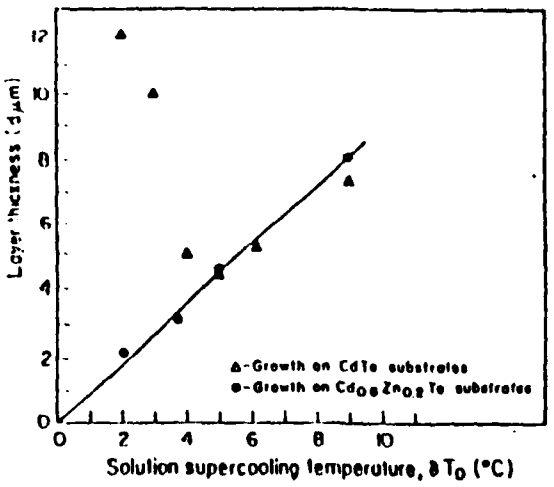

15. Variation of $Hg_{0.8}Zn_{0.2}Te$ epilayer thickness on growth time with the degree of supercooling of the growth solution. The solid line represent the empirical dependence on Te for the lattice matched case.

type	z	$-\Delta a/a$ x10-3	δTo °c	appearance	morphology	interface	C` μm/°c
I	0.2	≤1	2-9	mirror-like	typical LPE undulations	smooth	0.9
II	0-.04	10-14	>5	mat	rough	smooth	0.9
III	0-.18	2-14	3-4	mat	rough	undulant	1-4
IV	0-.04	10-14	2	mirror-like	triangular pattern on (111)B featureless on (111)A	fairly smooth	5

z Zn concentraion in the substrate
δTo The supercooling of the growth solution
C` The apparent prefix in exp. [1]
$\Delta a/a$ The lattice mismatch

Table II The various types of HgZnTe layers.

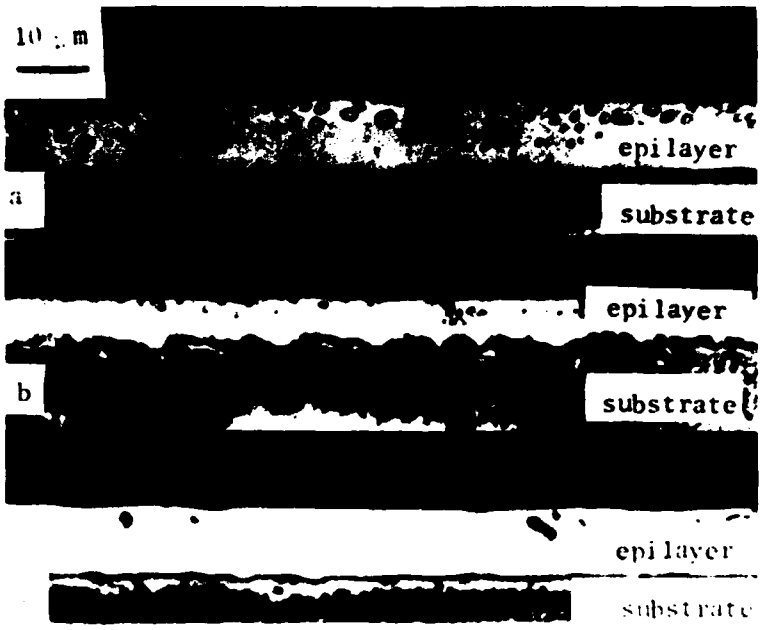

16. Scanning electron cleaved sections of $Hg_{0.8}Zn_{0.2}Te/CdTe$. The epilayers were grown with solution supercooling of: (a) 9°C; (b) 4°C; (c) 2°C.

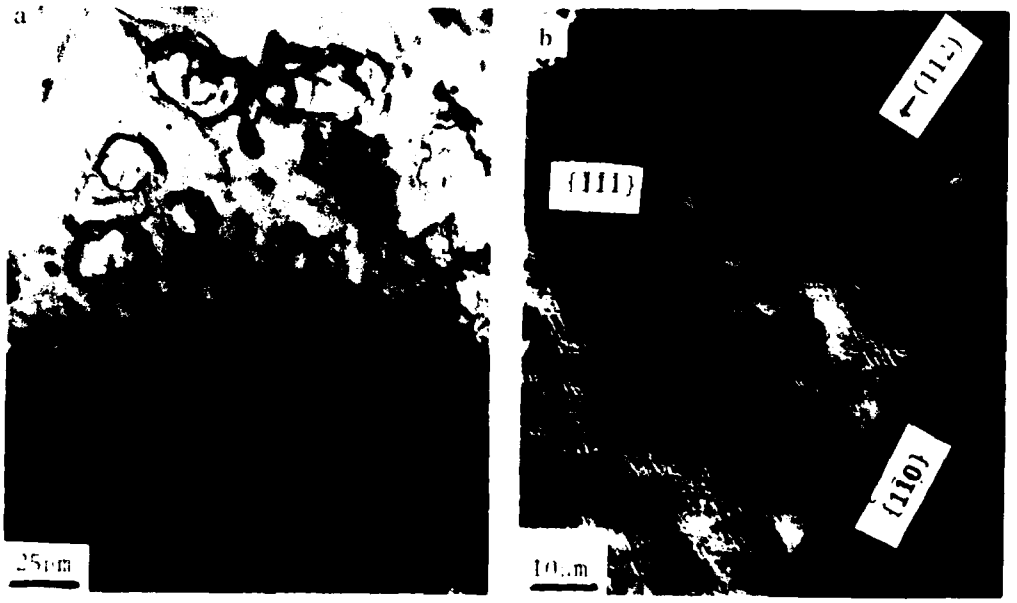

17. Typical morphology of $Hg_{0.8}Zn_{0.2}Te$ epilayers which were grown on CdTe substrates; (a) with δT_o = 9°C; (b) with δT_o = 2°C.

identical compositions. These three specific layers were grown on CdTe substrates. Similar results were found when the layers were grown on $Cd_{1-z}Zn_zTe$ substrates. The range of z typical to each category is notified in table II.

Type II epilayer, the interface of which is displayed in fig. (16a) was grown with supercooling of 9°C. In this case the interface is smooth. The result of the growth with a supercooling of 4°C, epilayer of type III, is seen in fig. (16b). The interface of that structure is undulant. The intrusions of the layer into the substrate are of the order of 2 microns. With supercooling of 2°C, the interface is again fairly smooth. Such an interface typical to layers of type IV is shown in fig. (16c). The morphologies of the epilayers of types II and IV are shown in fig. (17a) and (17b), respectively. The morphology typical to the layers of type II is very rough with high concentration of defects. Two kinds of morphologies were found in the layers which fall into the category of type IV. In fig. (17b), the morphology of a layer which was grown on (111)B face with δT=2°C is shown. A triangular-hatch pattern is clearly seen in this figure. The lines are in the [112] direction, parallel to the intersection lines between (110) planes and the (111)B, the plane of growth. Those layers which were grown on (111)A, under the same growth conditions exhibited almost featureless morphology. All the layers of type IV were mirror-like. In the layers of type I, grown on $Cd_{0.8}Zn_{0.2}Te$ substrates with lattice mismatch 1_x10^{-3} or less, the interfaces were smooth and the morphology had LPE undulations. The effect of changing δT_o on both was minor. Typical morphology of the type I epilayers has been shown in fig. (13a).

So far,all the observed phenomena were attributed to the lattice mismatch but, actually they could be caused by different concentrations of Zn in the substrates. In fig. (18) the results of the full width at the half maximum (FWHM) of the rocking curve spectra were plotted versus $\Delta a/a$, the lattice mismatch between the layer and the substrate. The FWHM is an indication of the influence of the mismatch on the crystalline quality of epitaxial layers (17). The divergence range of the FWHM for the various types is displayed in this figure. The general trend is clearly evident. With lattice mismatch less than $-1x10^{-3}$, typical to layers of type I, the FWHM was determined by the FWHM of the CdZnTe substrates, 80-100 arc seconds. With the largest lattice mismatch, around $-1x10^{-2}$, layers of types II and IV, the FWHM of the layers was 300 - 400 arc seconds with no

dependence on the growth conditions, nor on the chemical composition of the substrate. Similar sharpness of the IR absorption edges of the layers of types I, II indicated that there was not a difference in the compositional gradient which could lead to such widening of the FWHM (18). Thus it may be concluded that no matter in what processes the various types of the HgZnTe were formed, the crystalline quality was dependent only on the lattice mismatch.

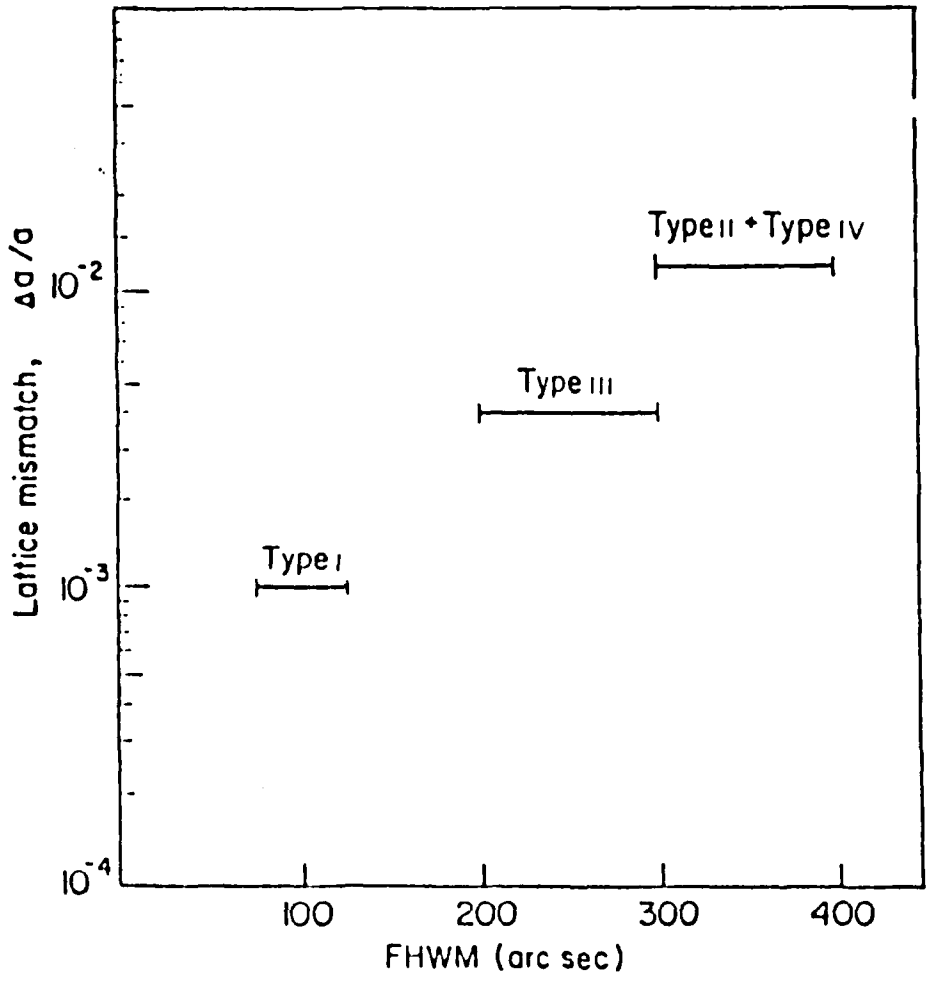

18. The divergence of the FWHM of $Hg_{0.8}Zn_{0.2}Te$ layers, related with various values of Δa/a.

5.4 The role of the strain energy in the LPE of HgZnTe epilayers

Interpreting the experimental phenomena, we follow the concept that at the initial stages of contact between the growth solution and the substrate, a "skin" which was in chemical equilibrium with the liquid was formed (19). In the case in which there was lattice mismatch, the "skin" was under stress. The critical thickness for introducing misfit dislocation in the II-VI heterostructures is less than 0.2 μm (20). It is reasonable to assume that the formation of misfit dislocation occurred a very short while after the "skin" was formed. In such a case there was no stage in which the liquid was "overheated" relative to a strained layer (21). Formation of micro cracks due to tension stresses, was found in many cases of vapor phase epitaxy of III-V compounds (22). The formation of such cracks was explained by pile-up of dislocations on the glide planes, terminated in cracking of the material (23). Evidence to the formation of micro cracks during LPE process of IV-VI (24) and II-VI heterostructures was also reported (25).

We suggest the formation of micro cracks in the tensiled "skin" of the HgZnTe solid solutions during the initial moments of the contact between the supercooled liquid and the substrate. In those cases in which the liquid remained in intimate contact with the "skin", the heat releasing which generally accompanies cracking of material (26) could cause the heating of the liquid at the interface. This overheating could cause in turn, meltback of the substrate. The formation of the various types of layers, presented in the precedent sections, can possibly be explained. Concerning the HgZnTe layers of type I in table II, in which the lattice mismatch was minimal, the distrubance to the LPE growth was minor. This led to epilayers having characteristics which were not strongly affected by the growth conditions. The quality of these epilayers was mainly determined by the substrate quality. Epilayers which fall into the category of type II in table II, were grown under large lattice mismatch and high degree of supercooling of the growth solution. Under such supercooling, the initial growth rate was enough to prevent, immediately, the contact between the substrate and the liquid. The strain energy could be relaxed through the introduction of structural defects, and no slowdown of the growth rate, induced by the lattice mismatch, could be detected. With the largest negative lattice mismatch but under the lowest supercooling of the growth solution, layers of type IV were formed. Under such conditions, the intentional supercooling was not high enough to

force thick overgrowth. Thus, the "skin" remained in intimate contact with the liquid. Assuming the formation of a high concentration of micro cracks in the tensiled HgZnTe "skin", the liquid was again in contact with the substrate, somewhat overheated due to the release of heat. Under such conditions, homogeneous meltback of the substrate was probable.

Such a process of "skin" formation, micro cracking and substrate meltback could last until the growth solution became supersaturated enough to force thick overgrowth on the "skin". The meltback of the substrate ceased and a regrowth process initiated. The "parallel" triangular hatch pattern was found to be typical to epilayers which were initiated in meltback followed by regrowth. Under intermediate lattice mismatch and supercooling layers of type III were formed. Under these conditions, it may be assumed that the layer exceeded only locally the critical thickness to prevent contact between the overheated liquid and the substrate. This situation could result in simultaneous meltback and regrowth. That was the origin of the undulant interfaces, typical to the layers of this category. The heterostructure $Hg_{0.8}Cd_{0.2}Te/CdTe$ can also fall into this category. This is in accordance with the irregularities frequently seen at the interface of that heterostructure (27).

In order to evaluate the potential of the strain energy to cause meltback, some assumptions have to be made. Returning to the results of the HgZnTe layers of type II, δT_2 can be taken as if it was the overheating of the growth solution due to the release of the strain energy. It is also assumed that there was dissolution of the substrate whenever $\delta T_2 > \delta T_o$. The amount of the dissolution is considered to be proportional to the difference between the strain energy induced overheating and the intentional supercooling, $\delta T_2 - \delta T_o$. As the meltback process was followed by regrowth of a relaxed layer, the final thickness had to be proportional to $\delta T_2 + \delta T_o$. Thus, the measured thickness had to be $C(\delta T_2 + \delta T_o)$. From the experimental results displayed in fig. (15), an approximate value to δT_2 could be evaluated, 10^oC for $\Delta a/a = -2 \times 10^{-2}$. In the same way δT_2 was evaluated for various values of $\Delta a/a$ while T_o was kept constant, 2^oC. As the strain energy should be proportional to $(\Delta a/a)^2$, $\delta T_2/T_3$ was plotted against this parameter, fig. (19). The triangulars are for growth runs performed with constant compositions of the growth solutions, appropriate for the growth of $Hg_{0.78}Zn_{0.22}Te$. The lattice mismatch in these growth runs was changed by altering the Zn concentration in the CdZnTe substrates. The circles are for growth runs of HgZnTe and HgCdTe with

compositions close to HgTe, on CdTe substrates. A theoretical line is also plotted in fig. (19). According to this theory the slowdown in the

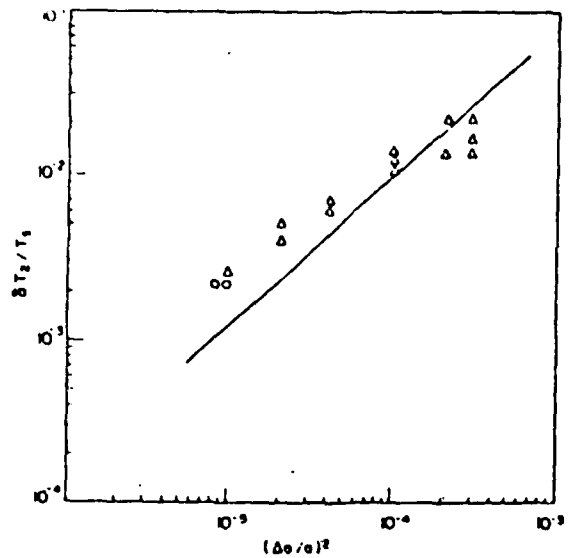

19. The amount of substrate meltback expressed by; $\delta T_2/T_s$, as a function of the square of the lattice mismatch. The line was calculated according to the theory presented in ref. 28.

Fig. 19

growth rate of garnet heterostructures, induced by the lattice mismatch, was explained (28). Considering δT_2 as the elevation in the saturation temperature, according to that theory:

$$\frac{\delta T_2}{T_s} = \frac{V Y (\Delta a/a)^2}{(1-\tau)} \qquad [3]$$

To plot the line, we chose Y, Young's modulus, 5×10^{11} dyne/cm^2, Poisson ratio, ν, 0.3, and τ, the heat of dissolution, 9000 cal/mole (29). V is the molar volume and T_s-the saturation temperature. The slight deviation from the theoretical slope is well understood if the introducing of Cd atoms into the growth solution during the meltback process is taken into consideration. It should be noted that for large positive lattice mismatch, for example when $Hg_{0.8}Cd_{0.2}Te$ was grown on a $Cd_{0.8}Zn_{0.2}Te$ substrate, the meltback was significantly less, as if $\delta T_2 = 0$. Thus, it turns out that without the mechanism of micro cracks which is significantly less probable under compressive stress, there is no lattice

mismatch induced meltback of the substrate. These results may confirm our basic hypothesis: the lattice mismatch was the factor which governed the substrate meltback and not the chemical incompatibility. We also suggest that the relaxation of the strain energy in the LPE of II-VI heterostructures, is via the formation of micro cracks, followed by meltback and regrowth processes.

5.5 Infrared transmission measurements

Transmission spectra of the HgZnTe epilayers, before and after the annealing process, are presented in fig. (20) and in fig. (21) respectively. It can be seen that as a result of the annealing process, the absolute transmission beyond the cut off wavelength reaches 54% which is the maximum transmission value considering the reflection losses (30). The range of the maximum transmission is also enlarged as a result of the annealing process. The steep decrease of the transmission at the longest wavenumbers seen in fig. (20), generally attributed to free carrier absorption, is not seen in transmission spectrum of the annealed samples. As it can be seen in fig. (22), the transmission spectra of sample HZ 73 (see table III) before and after the annealing process, the cut off wavelength itself was not changed due to the annealing process.

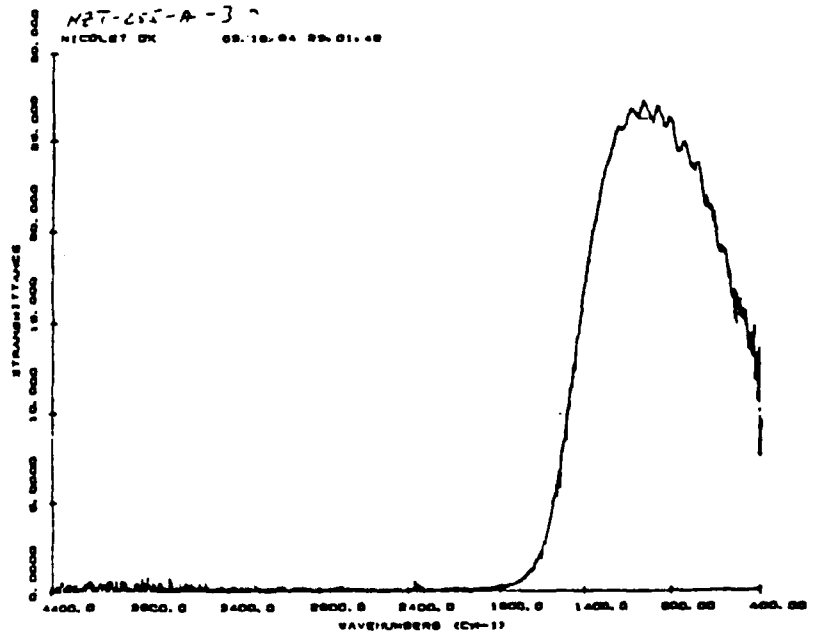

20. Typitcal transmission spectrum of an as grown HgZnTe epilayer.

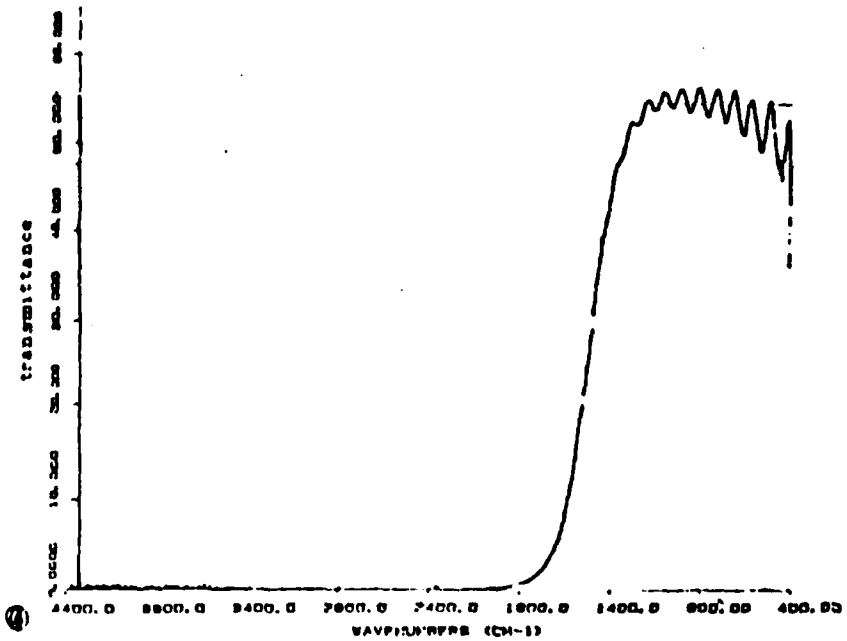

21. Typical transmission spectrum of an annealed HgZnTe epilayer.

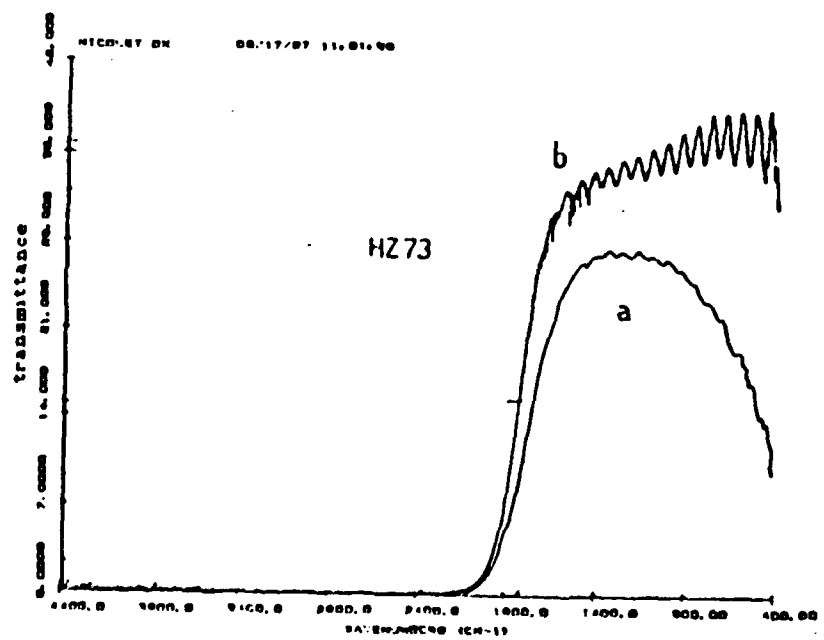

22. Change of the transmission spectrum of following the annealing process of epilayer HZ73 (see table III).

Table III

Data of annealed HgZnTe epilayers. The I-IV classification is according to table criteria. The electrical measurements performed at 80K.

Sample	x	type	Annealing conditions h	Annealing conditions T°C	R_H $\frac{cm^{-3}}{C}$	μ $\frac{cm^2}{VS}$	$\rho_{\Omega cm}$	$n/p \times 10^{16}$ cm^{-3}	
49A	0.18	III	16	400	+200	200	0.52	p3.5	
59B	0.18	III	48	300	+3	160	0.02	p200	
53	0.24	II	48	260	-300	1500	0.22	n1.6	
54	0.24	I-III	48	260	-500	4200	0.12	n1.2	
55	0.24	II	16	400	-530	60	6.1	n1.2	Continuous change between 1-10 KG
					-340	90	6.1	n1.8	
57	0.24	II-III	16	400	+55	120	0.47	p 11	
62	0.24	IV	16	400	-3	-46	0.06	n100	Continuous change between 1-10 KG
					-70	1170	0.08		
64A	0.24	IV	400			1.2			Non-consistent results with magnetic field
64B	0.24	IV	16	400					
73	0.21	I-III	16	400	+150	230	0.66	p 4	
84	0.17	I	16	400	+50	190	0.27	p 10	
85	0.21	I	16	360	+405	300	1.44	p1.5	
86	0.17	I	16	360	+420	340	1.25	p1.4	
89	0.17	I	16	360	+97	277	0.35	p 6	
90	0.17	I	48	340	+148	145	1.0	p 4	
91	0.17	I	16	360	+115	234	0.49	p 5	
92	0.17	I	16	360	+85	250	0.34	p 7	
110	0.17	I	16	360	+163	334	0.48	p 4	
113	0.17	I	72	260		9500		n	Continuous change between 1-10 KG
						6000			
114	0.16	I	72	260	+187	236	0.79	p 3	

5.6 The electrical transport measurements of annealed samples

As grown epilayers exhibited p-type conductivity with a hole concentration of $2\text{-}4\times10^{17}$ and hole mobility of 150-200 $cm^2V^{-1}sec^{-1}$. About twenty samples were annealed in Hg atmosphere, at temperatures lower than the growth temperature. The results of the electrical transport measurements of these samples are summarized in table III. Also notified in this table, the annealing conditions and the classification of the epilayers according the criteria of table II. When the category of the sample was ambiguous, the two relevant categories were denoted. All these samples were measured after removing about 2-3 microns of the surface by etching. Out of sixteen annealing experiments in which the ambient temperature was 340-400°C, only ten had been affected by the annealing process. In these samples the Hall constant was positive, not dependent on the magnetic field and with carrier concentration of $1\text{-}10\times10^{16}cm^{-3}$. Out of the samples categorized as types II and IV, only one sample had meaningful results after annealing. In all the other samples of these types the carrier concentration remained as high as in the as grown material or, R_H was negative with a strong and sometimes irregular dependence on the magnetic field. The results were the same also after deeper etching. It should be emphasized that due to their poor crystalline quality, only relative small number of samples of these types have been annealed. In fig. (23) the carrier concentration is presented as a function of the annealing temperature. It can be seen in this figure that in all the examined annealing temperatures, there were samples in which the carrier concentration decreased, as a result of the annealing process, to the level of $4\times10^{16}cm^{-3}$ or less. p type samples with the lowest carrier concentration were achieved at 360°C (annealing temperature). The hole concentrationin these samples was $1.5\times10^{16}cm^{-3}$ and the hole mobility was $350cm^2V^{-1}sec^{-1}$. These results may lead to the conclusion that the mechanism of diffusion of Hg into the epilayer and filling cations vacancies predominate the carrier concentration in HgZnTe in the same way generally assumed for HgCdTe (31). Other samples annealed at low temperature showed carrier concentration twice or more higher than the best results. It may be concluded that the annealing temperature is not the only factor which determines the carrier concentration, thus there ought to be another source of acceptors which is not the equilibrium cation vacancy concentration. Since such a source could be residual

impurities, some of the layers were measured by Secondary Ion Mass Spectrography (SIMS). Results are discussed in Section 5.7.

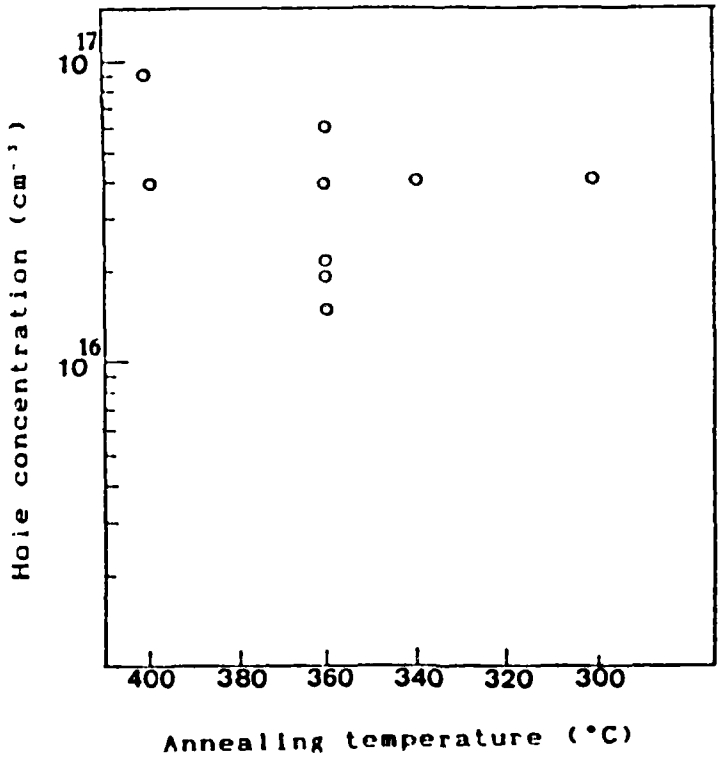

23. Carrier concentration at 80 K of HgZnTe epilayers as a function of the annealing temperature.

Fig. 23

5.7 Impurity depth profile by SIMS

HgZnTe epilayers, HZ49, HZ54 and HZ55 (see table III for the samples definition) were submitted to Charls Evans and Associates (32) for impurity depth profile analysis. Two annealed, p type $Hg_{0.8}Cd_{0.2}Te$ epilayers were also submitted for the depth profiling as a reference. The measured hole concentration in the HgCdTe epilayer was $1x10^{16}cm^{-3}$ and $5x10^{16}cm^{-3}$ in AN229 and AN233, respectively.

Cesium energetic ion bombardment and negative secondary ion mass spectrometry were employed to monitor Si, S, Se, and Te in the five epi layer samples. Oxygen ion bombardment and positive secondary ion mass spectrometry were employed to profile Li,Na, Mg, Al, Fe, Cu, Zn, In, Cd, Te, Hg, and Pb in a second area of each layer.

The real time ion intensity versus sputter time data has been processed to provide plots of concentration versus depth for the impurity elements of interest, and relative ion intensity versus depth for the matrix constituents. The conversion to a concentration scale is based on relative sensitivity factors (RSF's) derived from previous analysis of ion implant standards in HgCdTe and CdTe. The accuracy of the concentration scale is a factor of two in a HgCdTe matrix. The depth scale is calibrated with a sputter rate determined from a stylus profilometer measurement of each of the analytical sputtered craters. The depth scale is accurate of 10%. The Zn, Cd, Te, and Hg signals are used to delineate the layer structure and provide no quantitative information. Plots of the real time and parocessed data as well as expanded plots of the processed data have been provided for each profile.

No major differences were detected between sample to sample thus, only the SIMS results of the HgZnTe epilayer HZ-49 and the reference HgCdTe epilayer AN229 are presented. The depth profile of 3 nonmetal impurities is presented in fig. (24). In the two samples there is high concentration, above $10^{18}cm^{-3}$ of Si and S, at the surface, which drops to the low 10^{15} with the epilayer depth.

The depth profile of the metal impurities is presented in fig. (26). Of these impurities, Cu and Fe, both known as dopants in HgCdTe (32) were found in extremely high concentrations in all the five samples. High concentrtion of Pb were found only in part of the samples. Since such high concentrations of Cu, Fe and Pb were not consistent with the electrical measurements, repeat measurement of these three elements was performed in all the five samples. This time the "voltage offset" technique (33) was employed in order to reduce the matrix elements interference which could have been ther reason misleading results.

Using this technique, the results of the SIMS analysis, presented in fig. (27) are significantly different. The measured Cu concentration is at the 10^{16} level which may still be due to the background contribution to the Cu signals from molecular and multiply charge matrix ion species. A significant surface contamination in Fe is still observed. These results were also very similar in all the five samples.

While the SIMS results were not conclusive, the similarity between the SIMS results of all the samples, including the low p type HgCdTe epi ayer, indicates that there must be another source to the relative high hole concentration in HZ49 as well as in AN233. It is also indicated that as

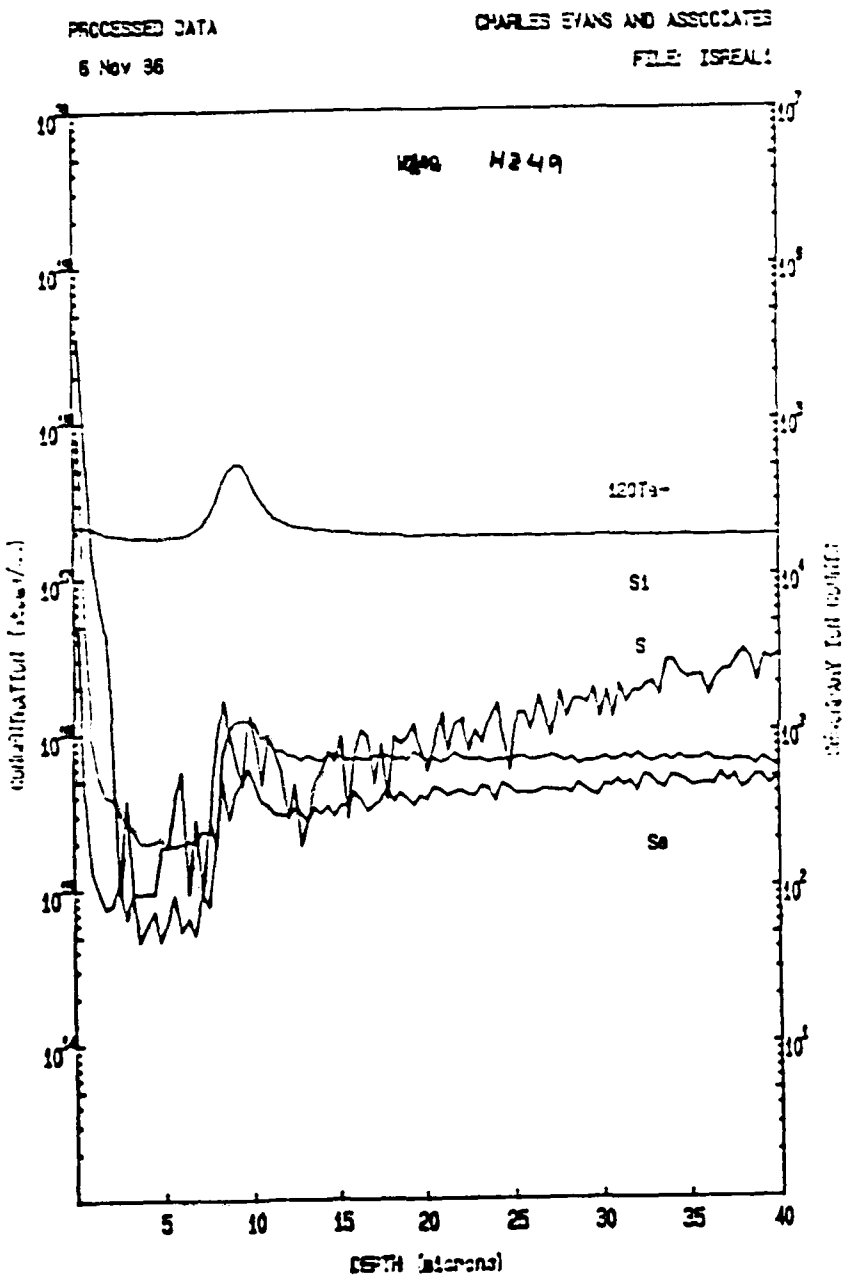

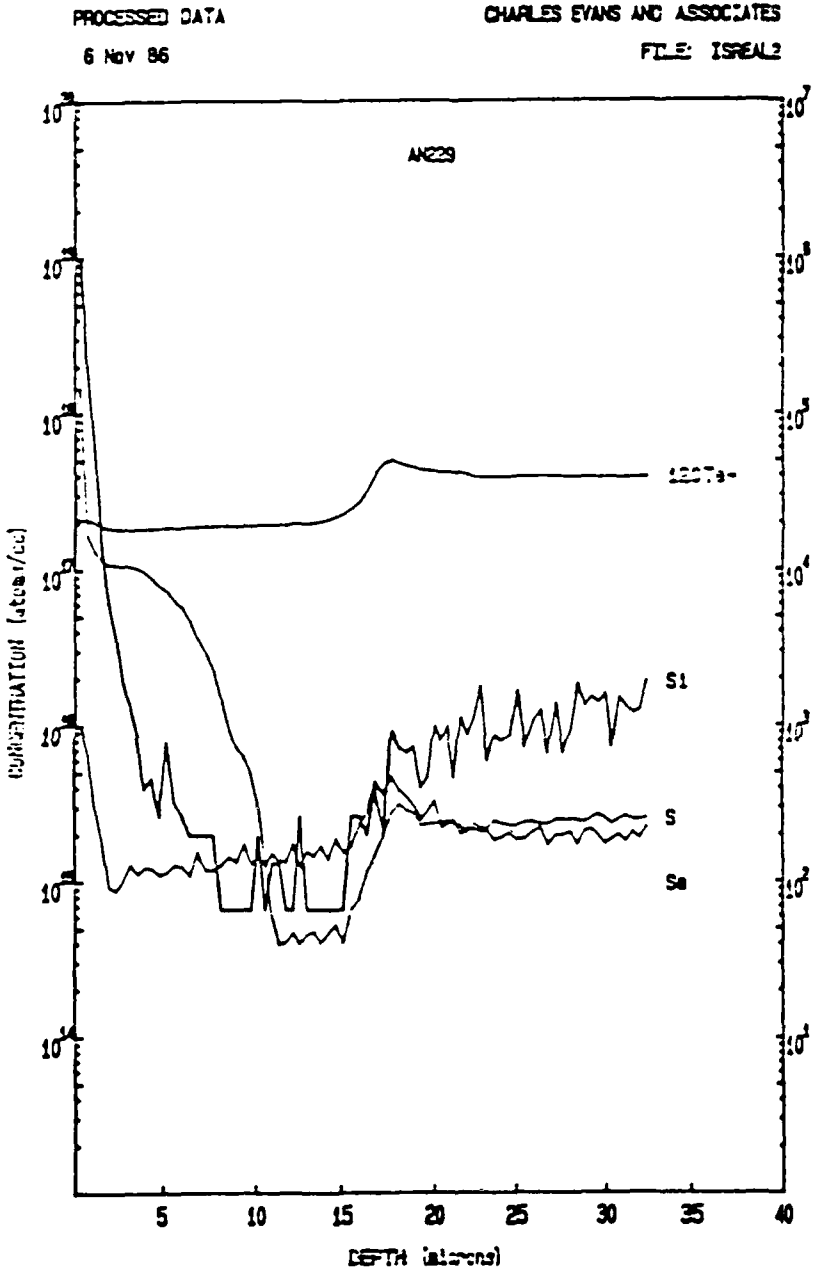

24. Depth profile by SIMS of 3 non metal impurities.

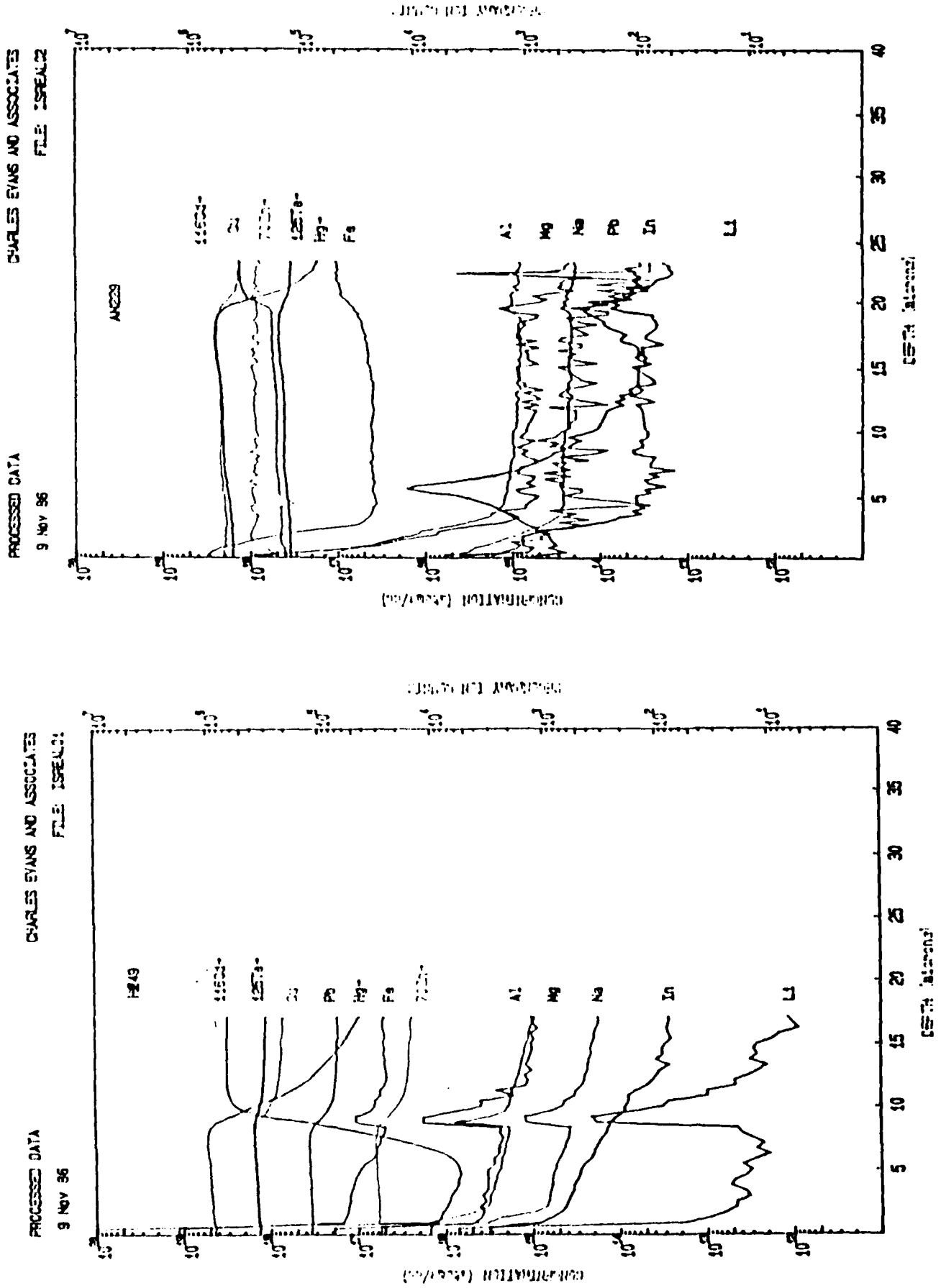

25. Depth profile by standard SIMS of metal impurities

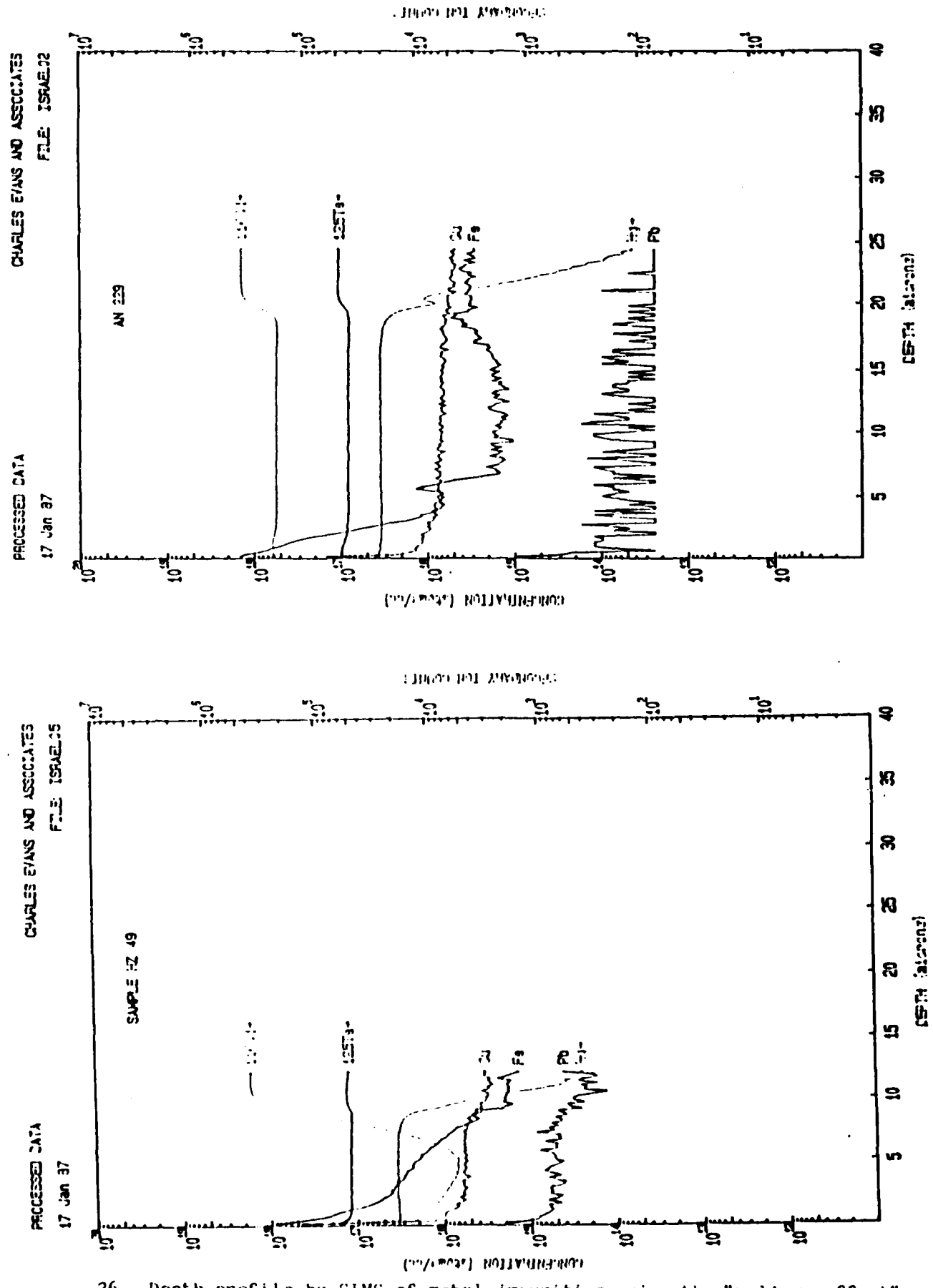

26. Depth profile by SIMS of metal impurities using the "voltage offset" technique.

there was no any impurity unique to the HgZnTe epilayers, the level of $1x10^{16}cm^{-3}$ can be reached.

5.8 Photoconductive spectral response measurements

The photoconductive spectral response of some of the annealed $Hg_{1-x}Zn_xTe$ epilayers was measured at 80K. The spectral response of sample HZ86 is presented in fig. (24). The photoconductive response started at 9μm and raised up to maximum at 4 μm. The steep drop at 6 μm and the discontinuity at 8 μm are instrumental.

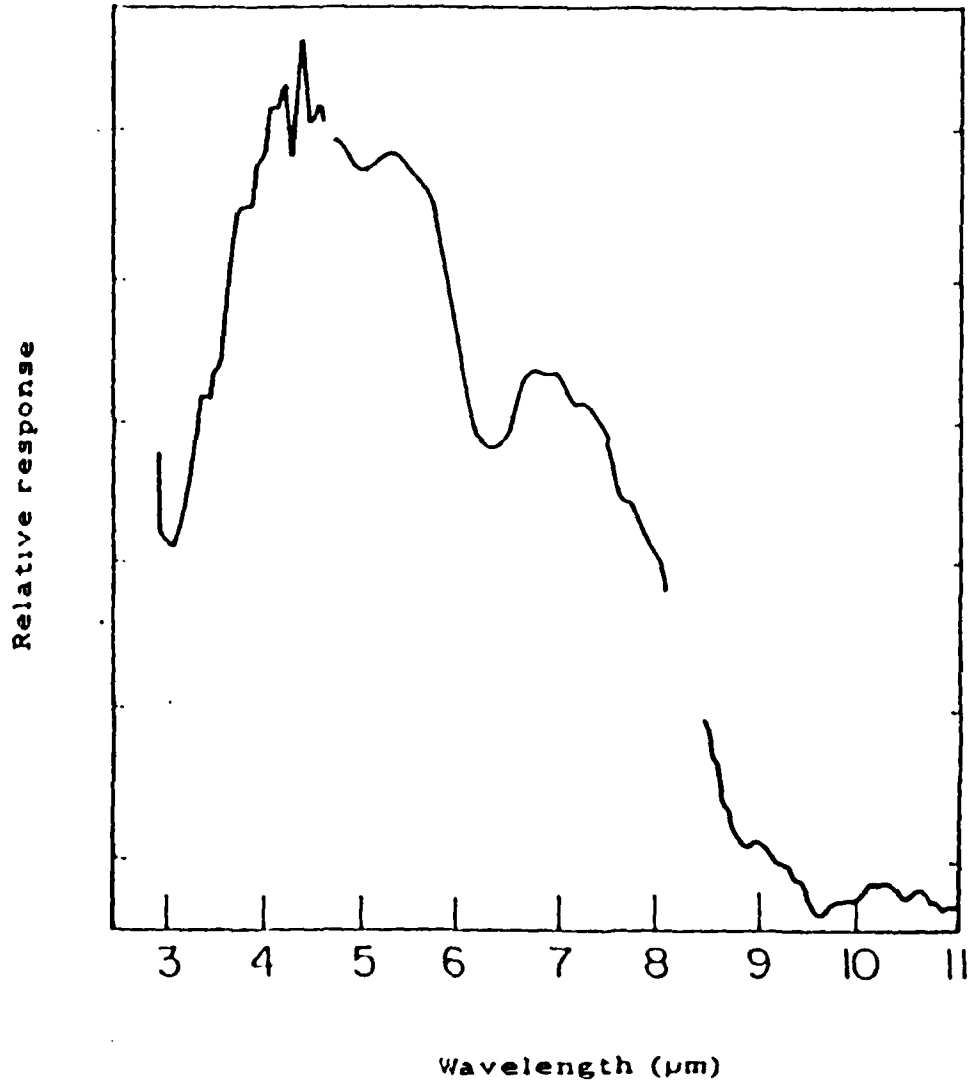

27. Photoconductive spectral response of HZ86 (see table III), at 80 K.

Fig. 27

6. Conclusions

The horizontal liquid phase epitaxy from Te solution of HgznTe, was studied systematically. The conditions in which the growth was diffusion limited were found. Optimizing the growth conditions, $Hg_{1-x}Zn_xTe$ epilayers $0.11<x<0.26$, with morphological and crystalline quality generally limited by the substrate quality, were grown. The lattice mismatch between the epilayer and the substrate was found to be a dominant factor governing the epilayer quality. It was found that the growth on CdTe or CdZnTe substrates, under lattice mismatch > $2x10^{-3}$ resulted in meltback-regrowth processes unless a relative high degree of growth solution supercooling was employed. In both cases the crystalline quality of the epilayer was poor. A model describing the role of the strain energy, originated from the lattice mismatch, in the LPE of HgZnTe layers was suggested. Since the as grown epilayers were p type with a carrier concentration $2-4x10^{17}cm^{-3}$, annealing in Hg atmosphere was employed in order to reduce it to the level of $1-3x10^{16}$, generally required for photovoltaic detectors. Successful results were partially achieved and only when the epilayers were grown on closely lattice matched substrates (layers of type I in our classification).

Impurity depth profile by secondary ion mass spectrography (SIMS), of HgZnTe layers was compared with that of HgCdTe p type epilayer in which low hole concentration was measured. Although not conclusive, this measurement has not revealed another source of acceptors other than Hg vacancies.

We described in this report the conditions in which HgZnTe epilayers, with properties comparable to those of HgCdTe, can be achieved by LPE technique. At this point it is possible to initiate a systematic study of HgZnTe epitaxial layers as a material for IR photon-detectors; in particular, p-n junction formation and surface passivation processes.

References

1. Arden Sher, An Ban Chen, W.E. Spicer and C-k Shie, J. Vac. Sci. Technol. A3 (1985) 105.
2. Ariel Sher, D. Eger and A. Zemel, Appl. Phys. Letters 46 (1985) 59.
3. Ariel Sher, D. Eger, H. Feldstein and A. Raizman, J. Crystal Growth 72 (1985) 108.
4. E.J. Smith, T. Tung, S. Sen. W.H. Konkel, J.B. James, V.B. Harper, B.F. Zuck and R.A. Cole, J. Vac. Sci. Technol. A5 (1987) 3043.
5. S. Sen, W.H. Koukel, R.A. Cole, T. Tung, J.B. James, E.J. Smith, V.B. Harper and B.F. Zuck, US Workshop on MCT, (San Diego 1986).
6. J.P. Faurie, J. Reno, S. Sivanathan, I.K. Sou, X. Chu, M. Boukerch and P.S. Wijewarnasuriysa, J. Vac. Sci. Technol. A4 (1986) 2067.
7. Data was given by Dr. H. Feldstein, SNRC.
8. A. Sher, H. Feldstein, A. Raizman and A. Tsigelman, 3rd interim submitted to the ERO, Contract DATA 45-85-C-0049, February, 1987.
9. S. Rotter, U. Lacchish and U. El-Hanany, J. Crystal Growth 73 (1985) 187.
10. Y.C. Lu, R.K. Route, D. Elwell and R.S. Feigelson, J. Vac. Sci. Technol. A3 (1985) 264.
11. L.J. Van der Pauw, Philips Res. 13 (1958) 1.
12. T.C. Harman, J. Electron. Mater. 9 (1980) 945.
13. R.L. Moon, J. Crystal Growth 27 (1974) 62.
14. J.J. Hsie in: Handbook on Semiconductors Vol. 3, Ed. S.P. Keller, (North-Holland, Amsterdam, 1980).
15. D.W. Shaw, J. Crystal Growth 62 (1983) 7.
16. D. Elweel and H.J. Scheel in: Crystal Growth from High Temperature Solutions (Academic Press NY, 1975).
17. S.B. Quadri and J.H. Dinan, Appl. Phys. Letters 47 (1985) 1066.
18. Ariel Sher, D. Eger, A. Zemel, H. Feldstein and A. Raizman, J. Vac. Sci. Technol. A4 (1985) 2024.
19. M.B. Small and R. Ghez, J. Appl. Phys. 50 (1979) 5322.
20. J.H. Basson and H. Booyens, Phys. Stat. Sol. 80 (1983) 663.
21. Yu, B. Bolkhvityanov, J. Crystal Growth 55 (1981) 591.
22. L.R. Dawson, J. Vac. Sci. Technol B4 (1986) 598.
23. J.W. Matthews and A.E. Blakesslee, J. Crystal Growth 29, (1975) 273.
24. S. Rotter, J. Electron. Matter. 15 (1986) 141.

25. Ariel Sher, A. Raizman and D. Eger, to be published in J. Crystal Growth, 1988.
26. F.K.N. Nabaro, Theory of Crystal Dislocations (Oxford, 1967).
27. M. Astles, G. Blackmore, V. Steward, P.C. Rodway and P. Kirton, J. Crystal Growth 80 (1987) 1.
28. V.F. Dorfman, S.A. Petrushinina and M.L. Shupergin, Thin Solid Films 62 (1979) 157.
29. C-H Su, P-K Liao, T. Tung and R.F. Brebrick, High Temp. Sci. 14 (1981) 181.
30. I. Rabinoviz, M.Sc. Thesis, Tel Aviv University, 1983.
31. M. Chu. J. Appl. Phys. 51 (1980) 5876.
32. Charles Evans and Associates, 30, Chesapeake Drive, Redwood City, California 94063.
33. Technical notes of Charls Evans and Associates (1981).